leukemia patients after hematopoietic stem cell transplantation. *Cancer Research*, **64**, 391–399.

Harashima, N., Tanosaki, R., Shimizu, Y., Kurihara, K., Masuda, T., Okamura, J. & Kannagi, M. (2005) Identification of two new HLA-A*1101-restricted tax epitopes recognized by cytotoxic T lymphocytes in an adult T-cell leukemia patient after hematopoietic stem cell transplantation. *Journal of Virology*, **79**, 10088–10092.

Hermine, O., Bouscary, D., Gessain, A., Turlure, P., Leblond, V., Franck, N., Buzyn-Veil, A., Rio, B., Macintyre, E., Dreyfus, F. & Bazarbachi, A. (1995) Brief report: treatment of adult T-cell leukemia-lymphoma with zidovudine and interferon alfa. *New England Journal of Medicine*, **332**, 1749–1751.

Hinuma, Y., Nagata, K., Hanaoka, M., Nakai, M., Matsumoto, T., Kinoshita, K.I., Shirakawa, S. & Miyoshi, I. (1981) Adult T-cell leukemia: antigen in an ATL cell line and detection of antibodies to the antigen in human sera. *Proceedings of the National Academy of Sciences of the United States of America*, **78**, 6476–6480.

Hishizawa, M., Imada, K., Kitawaki, T., Ueda, M., Kadowaki, N. & Uchiyama, T. (2004) Depletion and impaired interferon-alpha-producing capacity of blood plasmacytoid dendritic cells in human T-cell leukaemia virus type I-infected individuals. *British Journal of Haematology*, **125**, 568–575.

Hishizawa, M., Kanda, J., Utsunomiya, A., Taniguchi, S., Eto, T., Moriuchi, Y., Tanosaki, R., Kawano, F., Miyazaki, Y., Masuda, M., Nagafuji, K., Hara, M., Takanashi, M., Kai, S., Atsuta, Y., Suzuki, R., Kawase, T., Matsuo, K., Nagamura-Inoue, T., Kato, S., Sakamaki, H., Morishima, Y., Okamura, J., Ichinohe, T. & Uchiyama, T. (2010) Transplantation of allogeneic hematopoietic stem cells for adult T-cell leukemia: a nationwide retrospective study. *Blood*, **116**, 1369–1376.

Ishida, T. & Ueda, R. (2011) Immunopathogenesis of lymphoma: focus on CCR4. *Cancer Science*, **102**, 44–50.

Ishida, T., Joh, T., Uike, N., Yamamoto, K., Utsunomiya, A., Yoshida, S., Saburi, Y., Miyamoto, T., Takemoto, S., Suzushima, H., Tsukasaki, K., Nosaka, K., Fujiwara, H., Ishitsuka, K., Inagaki, H., Ogura, M., Akinaga, S., Tomonaga, M., Tobinai, K. & Ueda, R. (2012) Defucosylated anti-CCR4 monoclonal antibody (KW-0761) for relapsed adult T-cell leukemia-lymphoma: a multicenter phase II study. *Journal of Clinical Oncology*, **30**, 837–842.

Ishida, T., Hishizawa, M., Kato, K., Tanosaki, R., Fukuda, T., Takatsuka, Y., Eto, T., Miyazaki, Y., Hidaka, M., Uike, N., Miyamoto, T., Tsudo, M., Sakamaki, H., Morishima, Y., Suzuki, R. & Utsunomiya, A. (2013) Impact of graft-versus-host disease on allogeneic hematopoietic cell transplantation for adult T cell leukemia-lymphoma focusing on preconditioning regimens: nationwide retrospective study. *Biology of Blood and Marrow Transplantation*, **19**, 1731–1739.

Jacobson, S., Shida, H., McFarlin, D.E., Fauci, A.S. & Koenig, S. (1990) Circulating CD8+ cytotoxic T lymphocytes specific for HTLV-I pX in patients with HTLV-I associated neurological disease. *Nature*, **348**, 245–248.

Jones, K.S., Petrow-Sadowski, C., Huang, Y.K., Bertolette, D.C. & Ruscetti, F.W. (2008) Cell-free HTLV-1 infects dendritic cells leading to transmission and transformation of CD4(+) T cells. *Nature Medicine*, **14**, 429–436.

Kannagi, M., Shida, H., Igarashi, H., Kuruma, K., Murai, H., Aono, Y., Maruyama, I., Osame, M., Hattori, T., Inoko, H. & Harada, S. (1992) Target epitope in the Tax protein of human T-cell leukemia virus type I recognized by class I major histocompatibility complex-restricted cytotoxic T cells. *Journal of Virology*, **66**, 2928–2933.

Katsuya, H., Yamanaka, T., Ishitsuka, K., Utsunomiya, A., Sasaki, H., Hanada, S., Eto, T., Moriuchi, Y., Saburi, Y., Miyahara, M., Sueoka, E., Uike, N., Yoshida, S., Yamashita, K., Tsukasaki, K., Suzushima, H., Ohno, Y., Matsuoka, H., Jo, T., Suzumiya, J. & Tamura, K. (2012) Prognostic index for acute- and lymphoma-type adult T-cell leukemia/lymphoma. *Journal of Clinical Oncology*, **30**, 1635–1640.

Kurihara, K., Harashima, N., Hanabuchi, S., Masuda, M., Utsunomiya, A., Tanosaki, R., Tomonaga, M., Ohashi, T., Hasegawa, A., Masuda, T., Okamura, J., Tanaka, Y. & Kannagi, M. (2005) Potential immunogenicity of adult T cell leukemia cells in vivo. *International Journal of Cancer*, **114**, 257–267.

Lee, B., Tanaka, Y. & Tozawa, H. (1989) Monoclonal antibody defining tax protein of human T-cell leukemia virus type-I. *The Tohoku Journal of Experimental Medicine*, **157**, 1–11.

Linette, G.P., Zhang, D., Hodi, F.S., Jonasch, E.P., Longerich, S., Stowell, C.P., Webb, I.J., Daley, H., Soiffer, R.J., Cheung, A.M., Eapen, S.G., Fee, S.V., Rubin, K.M., Sober, A.J. & Haluska, F.G. (2005) Immunization using autologous dendritic cells pulsed with the melanoma-associated antigen gp100-derived G280-9V peptide elicits CD8+ immunity. *Clinical Cancer Research*, **11**, 7692–7699.

Makino, M., Wakamatsu, S., Shimokubo, S., Arima, N. & Baba, M. (2000) Production of functionally deficient dendritic cells from HTLV-I-infected monocytes: implications for the dendritic cell defect in adult T cell leukemia. *Virology*, **274**, 140–148.

Nagayama, H., Sato, K., Morishita, M., Uchimaru, K., Oyaizu, N., Inazawa, T., Yamasaki, T., Enomoto, M., Nakaoka, T., Nakamura, T., Maekawa, T., Yamamoto, A., Shimada, S., Saida, T., Kawakami, Y., Asano, S., Tani, K., Takahashi, T.A. & Yamashita, N. (2003) Results of a phase I clinical study using autologous tumour lysate-pulsed monocyte-derived mature dendritic cell vaccinations for stage IV malignant melanoma patients combined with low dose interleukin-2. *Melanoma Research*, **13**, 521–530.

Ohashi, T., Hanabuchi, S., Kato, H., Tateno, H., Takemura, F., Tsukahara, T., Koya, Y., Hasegawa, A., Masuda, T. & Kannagi, M. (2000) Prevention of adult T-cell leukemia-like lymphoproliferative disease in rats by adoptively transferred T cells from a donor immunized with human T-cell leukemia virus type 1 Tax-coding DNA vaccine. *Journal of Virology*, **74**, 9610–9616.

Okamura, J., Utsunomiya, A., Tanosaki, R., Uike, N., Sonoda, S., Kannagi, M., Tomonaga, M., Harada, M., Kimura, N., Masuda, M., Kawano, F., Yufu, Y., Hattori, H., Kikuchi, H. & Saburi, Y. (2005) Allogeneic stem-cell transplantation with reduced conditioning intensity as a novel immunotherapy and antiviral therapy for adult T-cell leukemia/lymphoma. *Blood*, **105**, 4143–4145.

Poiesz, B.J., Ruscetti, F.W., Gazdar, A.F., Bunn, P.A., Minna, J.D. & Gallo, R.C. (1980) Detection and isolation of type C retrovirus particles from fresh and cultured lymphocytes of a patient with cutaneous T-cell lymphoma. *Proceedings of the National Academy of Sciences of the United States of America*, **77**, 7415–7419.

Rende, F., Cavallari, I., Corradin, A., Silic-Benussi, M., Toulza, F., Toffolo, G.M., Tanaka, Y., Jacobson, S., Taylor, G.P., D'Agostino, D.M., Bangham, C.R. & Ciminale, V. (2011) Kinetics and intracellular compartmentalization of HTLV-1 gene expression: nuclear retention of HBZ mRNAs. *Blood*, **117**, 4855–4859.

Takamori, A., Hasegawa, A., Utsunomiya, A., Maeda, Y., Yamano, Y., Masuda, M., Shimizu, Y., Tamai, Y., Sasada, A., Zeng, N., Choi, I., Uike, N., Okamura, J., Watanabe, T., Masuda, T. & Kannagi, M. (2011) Functional impairment of Tax-specific but not cytomegalovirus-specific CD8+ T lymphocytes in a minor population of asymptomatic human T-cell leukemia virus type 1-carriers. *Retrovirology*, **8**, 100.

Takeda, S., Maeda, M., Morikawa, S., Taniguchi, Y., Yasunaga, J., Nosaka, K., Tanaka, Y. & Matsuoka, M. (2004) Genetic and epigenetic inactivation of tax gene in adult T-cell leukemia cells. *International Journal of Cancer*, **109**, 559–567.

Tanosaki, R., Uike, N., Utsunomiya, A., Saburi, Y., Masuda, M., Tomonaga, M., Eto, T., Hidaka, M., Harada, M., Choi, I., Yamanaka, T., Kannagi, M., Matsuoka, M. & Okamura, J. (2008) Allogeneic hematopoietic stem cell transplantation using reduced-intensity conditioning for adult T cell leukemia/lymphoma: impact of antithymocyte globulin on clinical outcome. *Biology of Blood and Marrow Transplantation*, **14**, 702–708.

Thomas-Kaskel, A.K., Zeiser, R., Jochim, R., Robbel, C., Schultze-Seemann, W., Waller, C.F. & Veelken, H. (2006) Vaccination of advanced prostate cancer patients with PSCA and PSA peptide-loaded dendritic cells induces DTH responses that correlate with superior overall survival. *International Journal of Cancer*, **119**, 2428–2434.

Tsukasaki, K., Hermine, O., Bazarbachi, A., Ratner, L., Ramos, J.C., Harrington, W. Jr, O'Mahony, D., Janik, J.E., Bittencourt, A.L., Taylor, G.P., Yamaguchi, K., Utsunomiya, A., Tobinai, K. & Watanabe, T. (2009) Definition, prognostic

factors, treatment, and response criteria of adult T-cell leukemia-lymphoma: a proposal from an international consensus meeting. *Journal of Clinical Oncology*, **27**, 453–459.

Tsukasaki, K., Tobinai, K., Hotta, T. & Shimoyama, M. (2012) Lymphoma study group of JCOG. *Japanese Journal of Clinical Oncology*, **42**, 85–95.

Uchiyama, T., Yodoi, J., Sagawa, K., Takatsuki, K. & Uchino, H. (1977) Adult T-cell leukemia: clinical and hematologic features of 16 cases. *Blood*, **50**, 481–492.

Ueda, Y., Itoh, T., Nukaya, I., Kawashima, I., Okugawa, K., Yano, Y., Yamamoto, Y., Naitoh, K., Shimizu, K., Imura, K., Fuji, N., Fujiwara, H., Ochiai, T., Itoi, H., Sonoyama, T., Hagiwara, A., Takesako, K. & Yamagishi, H. (2004) Dendritic cell-based immunotherapy of cancer with carcinoembryonic antigen-derived, HLA-A24-restricted CTL epitope: clinical outcomes of 18 patients with metastatic gastrointestinal or lung adenocarcinomas. *International Journal of Oncology*, **24**, 909–917.

Utsunomiya, A., Miyazaki, Y., Takatsuka, Y., Hanada, S., Uozumi, K., Yashiki, S., Tara, M., Kawano, F., Saburi, Y., Kikuchi, H., Hara, M., Sao, H., Morishima, Y., Kodera, Y., Sonoda, S. & Tomonaga, M. (2001) Improved outcome of adult T cell leukemia/lymphoma with allogeneic hematopoietic stem cell transplantation. *Bone Marrow Transplantation*, **27**, 15–20.

Wierecky, J., Muller, M.R., Wirths, S., Halder-Oehler, E., Dorfel, D., Schmidt, S.M., Hantschel, M., Brugger, W., Schroder, S., Horger, M.S., Kanz, L. & Brossart, P. (2006) Immunologic and clinical responses after vaccinations with peptide-pulsed dendritic cells in metastatic renal cancer patients. *Cancer Research*, **66**, 5910–5918.

Wu, L., Adams, M., Carter, T., Chen, R., Muller, G., Stirling, D., Schafer, P. & Bartlett, J.B. (2008) lenalidomide enhances natural killer cell and monocyte-mediated antibody-dependent cellular cytotoxicity of rituximab-treated CD20+ tumor cells. *Clinical Cancer Research*, **14**, 4650–4657.

HTLV-1 induces a Th1-like state in CD4$^+$CCR4$^+$ T cells

Natsumi Araya,[1] Tomoo Sato,[1] Hitoshi Ando,[1] Utano Tomaru,[2] Mari Yoshida,[3] Ariella Coler-Reilly,[1] Naoko Yagishita,[1] Junji Yamauchi,[1] Atsuhiko Hasegawa,[4] Mari Kannagi,[4] Yasuhiro Hasegawa,[5] Katsunori Takahashi,[1] Yasuo Kunitomo,[1] Yuetsu Tanaka,[6] Toshihiro Nakajima,[7,8] Kusuki Nishioka,[7] Atae Utsunomiya,[9] Steven Jacobson,[10] and Yoshihisa Yamano[1]

[1]Department of Rare Diseases Research, Institute of Medical Science, St. Marianna University School of Medicine, Kanagawa, Japan. [2]Department of Pathology, Hokkaido University Graduate School of Medicine, Hokkaido, Japan. [3]Institute for Medical Science of Aging, Aichi Medical University, Aichi, Japan. [4]Department of Immunotherapeutics, Tokyo Medical and Dental University, Graduate School, Tokyo, Japan. [5]Department of Neurology, St. Marianna University School of Medicine, Kanagawa, Japan. [6]Department of Immunology, Graduate School of Medicine, University of the Ryukyus, Okinawa, Japan. [7]Institute of Medical Science and [8]Center for Clinical Research, Tokyo Medical University, Tokyo, Japan. [9]Department of Hematology, Imamura Bun-in Hospital, Kagoshima, Japan. [10]Viral Immunology Section, Neuroimmunology Branch, National Institutes of Health, Bethesda, Maryland, USA.

Human T-lymphotropic virus type 1 (HTLV-1) is linked to multiple diseases, including the neuroinflammatory disease HTLV-1–associated myelopathy/tropical spastic paraparesis (HAM/TSP) and adult T cell leukemia/lymphoma. Evidence suggests that HTLV-1, via the viral protein Tax, exploits CD4$^+$ T cell plasticity and induces transcriptional changes in infected T cells that cause suppressive CD4$^+$CD25$^+$CCR4$^+$ Tregs to lose expression of the transcription factor FOXP3 and produce IFN-γ, thus promoting inflammation. We hypothesized that transformation of HTLV-1–infected CCR4$^+$ T cells into Th1-like cells plays a key role in the pathogenesis of HAM/TSP. Here, using patient cells and cell lines, we demonstrated that Tax, in cooperation with specificity protein 1 (Sp1), boosts expression of the Th1 master regulator T box transcription factor (T-bet) and consequently promotes production of IFN-γ. Evaluation of CSF and spinal cord lesions of HAM/TSP patients revealed the presence of abundant CD4$^+$CCR4$^+$ T cells that coexpressed the Th1 marker CXCR3 and produced T-bet and IFN-γ. Finally, treatment of isolated PBMCs and CNS cells from HAM/TSP patients with an antibody that targets CCR4$^+$ T cells and induces cytotoxicity in these cells reduced both viral load and IFN-γ production, which suggests that targeting CCR4$^+$ T cells may be a viable treatment option for HAM/TSP.

Introduction

The flexibility of the CD4$^+$ T cell differentiation program that underlies the success of the adaptive immune response has recently been implicated in the pathogeneses of numerous inflammatory diseases (1–3). The majority of CD4$^+$ T lymphocytes belong to a class of cells known as Th cells, so called because they provide help on the metaphorical immune battlefield by stimulating the other soldiers — namely, B cells and cytotoxic T lymphocytes — via secretion of various cytokines. Interestingly, there is also a minority group of CD4$^+$ T cells with quite the opposite function: Tregs actively block immune responses by suppressing the activities of CD4$^+$ Th cells as well as many other leukocytes (4). Tregs are credited with maintaining immune tolerance and preventing inflammatory diseases that could otherwise occur as a result of uninhibited immune reactions (5). Thus, the up- or downregulation of certain CD4$^+$ T cell lineages could disrupt the carefully balanced immune system, threatening bodily homeostasis.

The plasticity of CD4$^+$ T cells, particularly Tregs, makes CD4$^+$ T cell lineages less clean-cut than they may originally appear. CD4$^+$ T cells are subdivided according to various lineage-specific chemokine receptors and transcription factors they express, as well as the cytokines they produce (6). Th1 cells, for example, can be identified by expression of CXC motif receptor 3 (CXCR3) and T box transcription factor (T-bet; encoded by *TBX21*) and are known to secrete the proinflammatory cytokine IFN-γ (6). While both have been known to express CC chemokine receptor 4 (CCR4) and CD25, Th2 cells and Tregs can usually be distinguished from each other by their expression of GATA-binding protein 3 (GATA3) and forkhead box p3 (FOXP3), respectively (6, 7). CCR4 is coexpressed in the majority of CD4$^+$FOXP3$^+$ cells and in virtually all CD4$^+$CD25$^+$FOXP3$^+$ cells, making it a useful — albeit not fully specific — marker for Tregs (8, 9). FOXP3 is a particularly noteworthy marker because its expression is said to be required for Treg identity and function (10). In fact, *Foxp3* point mutations are reported to cause fatal multiorgan autoimmune diseases (11). Even partial loss of FOXP3 expression can disrupt the suppressive nature of Tregs, representing one of several pathways by which even fully differentiated Tregs can reprogram into inflammatory cells (12). There have been several reports of Tregs reprogramming in response to proinflammatory cytokines such as IL-1, IL-6, IL-12, and IFN-γ (12, 13); it is thought that this reprogramming may have evolved as an adaptive mechanism for dampening immune suppression when protective inflammation is necessary (12). However, this same plasticity can lead to pathologically chronic inflammation, and several autoimmune diseases have been associated with reduced FOXP3 expression and/or Treg function, including multiple sclerosis, myasthenia gravis, and type 1 diabetes (14, 15).

Of the roughly 10–20 million people worldwide infected with human T-lymphotropic virus type 1 (HTLV-1), up to 2%–3% are affected by the neurodegenerative chronic inflammatory dis-

Conflict of interest: The authors have declared that no conflict of interest exists.
Submitted: January 17, 2014; **Accepted:** May 8, 2014.
Reference information: *J Clin Invest.* 2014;124(8):3431–3442. doi:10.1172/JCI75250.

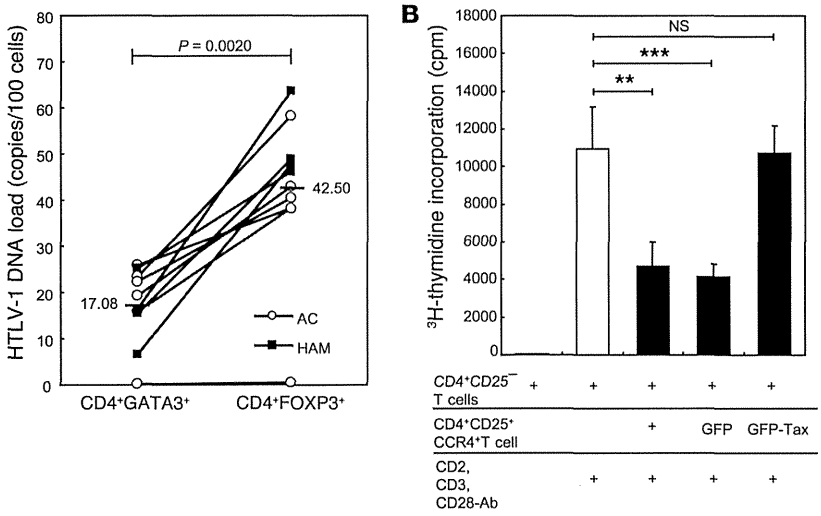

Figure 1. HTLV-1 mainly infects Tregs and inhibits their regulatory function. (**A**) Higher HTLV-1 proviral DNA load in CD4⁺FOXP3⁺ cells (Tregs) compared with CD4⁺GATA3⁺ cells ($P = 0.0020$, Wilcoxon test) from asymptomatic carriers (AC; $n = 6$) and HAM/TSP patients ($n = 4$). PBMCs were FACS sorted, and proviral load was measured using quantitative PCR. Horizontal bars represent the mean value for each set. (**B**) Loss of regulatory function in Tax-expressing CD4⁺CD25⁺CCR4⁺ cells (Tregs). CD4⁺CD25⁻ T cells from an HD were stimulated with CD2, CD3, and CD28 antibodies and cultured alone or in the presence of equal numbers of CD4⁺CD25⁺CCR4⁺ T cells, GFP lentivirus–infected HD CD4⁺CD25⁺CCR4⁺ T cells, or GFP-Tax lentivirus–infected HD CD4⁺CD25⁺CCR4⁺ T cells. As a control, CD4⁺CD25⁻ T cells alone were cultured without any stimulus. Proliferation of T cells was determined using ^{3}H-thymidine incorporation by adding ^{3}H-thymidine for 16 hours after 4 days of culture. All tests were performed in triplicate. Data are mean ± SD. $^{**}P < 0.01$, $^{***}P < 0.001$, ANOVA followed by Tukey test for multiple comparisons.

ease HTLV-1–associated myelopathy/tropical spastic paraparesis (HAM/TSP). The main other condition associated with the retrovirus is adult T cell leukemia/lymphoma (ATLL), a rare and aggressive cancer of the T cells. HAM/TSP represents a useful starting point from which to investigate the origins of chronic inflammation, because the primary cause of the disease — viral infection — is so unusually well defined. HAM/TSP patients share many immunological characteristics with FOXP3 mutant mice, including multiorgan lymphocytic infiltrates, overproduction of inflammatory cytokines, and spontaneous lymphoproliferation of cultured CD4⁺ T cells (16–18). We and others have proposed that HTLV-1 preferentially infects CD4⁺CD25⁺CCR4⁺ T cells, a group that includes Tregs (7, 19). Samples of CD4⁺CD25⁺CCR4⁺ T cells isolated from HAM/TSP patients exhibited low FOXP3 expression as well as reduced production of suppressive cytokines and low overall suppressive ability — in fact, these CD4⁺CD25⁺CCR4⁺FOXP3⁻ T cells were shown to produce IFN-γ and express Ki67, a marker of cell proliferation (19). The frequency of these IFN-γ–producing CD4⁺CD25⁺CCR4⁺ T cells in HAM/TSP patients was correlated with disease severity (19). Finally, evidence suggests that the HTLV-1 protein product Tax may play a role in this alleged transformation of Tregs into proinflammatory cells in HAM/TSP patients: transfecting Tax into CD4⁺CD25⁺ cells from healthy donors (HDs) reduced FOXP3 mRNA expression, and Tax expression in CD4⁺CD25⁺CCR4⁺ cells was higher in HAM/TSP versus ATLL patients despite similar proviral loads (19, 20). Therefore, we hypothesized that HTLV-1 causes chronic inflammation by infecting CD4⁺CD25⁺CCR4⁺ T cells and inducing their transformation into Th1-like, IFN-γ–producing proinflammatory cells via intracellular Tax expression and subsequent transcriptional alterations including but not limited to loss of endogenous FOXP3 expression.

In this study, we first sought to discover the detailed mechanism by which Tax influences the function of CD4⁺CD25⁺CCR4⁺ T cells. We used DNA microarray analysis of CD4⁺CD25⁺CCR4⁺ T cells from HAM/TSP patients to identify *TBX21*, known as a master transcription factor for Th1 differentiation, as a key intermediary between Tax expression and IFN-γ production. We demonstrated that Tax, in concert with specificity protein 1 (Sp1), amplified *TBX21* transcription and subsequently IFN-γ production. Next, we established the presence of Th1-like CD4⁺CCR4⁺ T cells in the CSF and spinal cord lesions of HAM/TSP patients. The majority of these CD4⁺CCR4⁺ T cells coexpressed CXCR3 as well as T-bet and IFN-γ. Finally, we investigated the therapeutic potential of an anti-CCR4 monoclonal antibody with antibody-dependent cellular cytotoxicity (ADCC) (21). Applying this antibody in vitro diminished the proliferative capacity of cultured PBMCs and reduced both proviral DNA load and IFN-γ production in cultured CSF cells as well as PBMCs. In conclusion, we were able to elucidate a more detailed mechanism for the pathogenesis of HAM/TSP and use our findings to suggest a possible therapeutic strategy.

Results

HTLV-1 preferentially infects Tregs and alters their behavior via Tax. Experiments were conducted to determine which among CD4⁺CD25⁺CCR4⁺ T cells were infected by HTLV-1, and how the infection influenced their functionality. Analysis of fluorescence-activated cell sorting (FACS)-sorted PBMCs obtained from asymptomatic carriers ($n = 6$) as well as HAM/TSP patients ($n = 4$) revealed that Tregs (CD4⁺FOXP3⁺) carried much higher proviral loads than Th2 cells (CD4⁺GATA3⁺) ($P = 0.0020$; Figure 1A). As it is well established that each infected cell contains only 1 copy of the HTLV-1 provirus (22, 23), these results indicate that a larger proportion of FOXP3⁺ than GATA3⁺ CD4⁺ T cells are infected. As expected, proliferation of CD4⁺CD25⁻ cells after stimulation, as measured by ^{3}H-thymidine incorporation, was suppressed upon coculture with CD4⁺CD25⁺CCR4⁺ cells, including Tregs ($n = 3$, $P < 0.01$; Figure 1B). However, after being transduced with lentiviral vector expressing GFP-Tax, the CD4⁺CD25⁺CCR4⁺ cells no longer suppressed cell proliferation; conversely, cells transduced with the control vector expressing only GFP retained full suppressive function ($P < 0.001$; Figure 1B).

The HTLV-1 protein product Tax induces IFN-γ production via T-bet. Experiments were conducted to determine if and how Tax affects IFN-γ production in infected T cells. First, the existence of a functional link between *Tax* and *IFNG* was established by using the

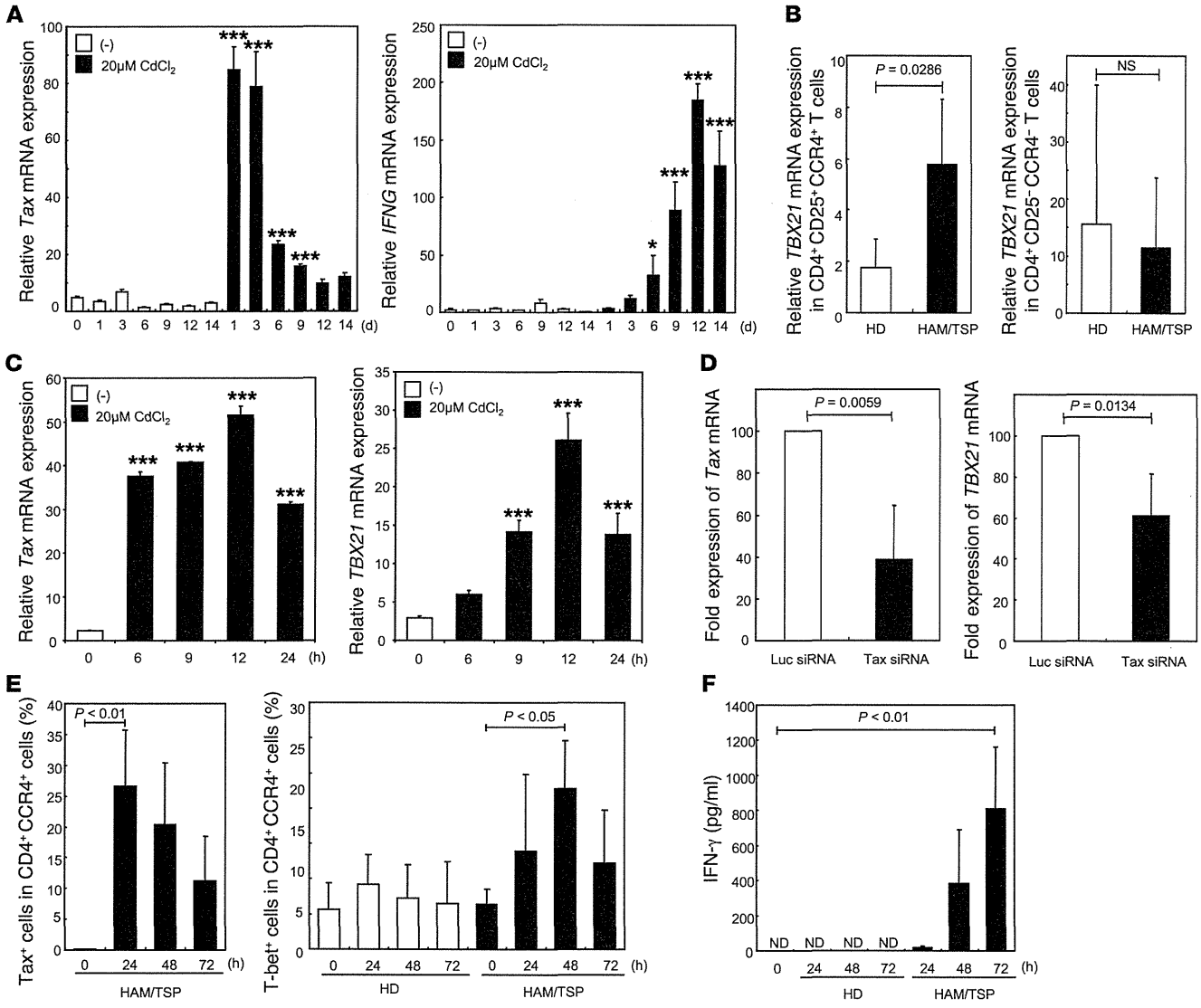

Figure 2. Tax induces IFN-γ production via T-bet. (**A**) Tax-dependent *IFNG* mRNA expression in JPX-9 cells. Experiments were performed in triplicate. (**B**) Elevated *TBX21* mRNA expression in CD4⁺CD25⁺CCR4⁺ T cells from HAM/TSP patients relative to HDs (n = 4 per group). (**C**) Tax-dependent *TBX21* mRNA expression in JPX-9 cells. Experiments were performed in triplicate. (**D**) Reduced *TBX21* mRNA expression after silencing Tax in CD4⁺CD25⁺CCR4⁺ T cells from HAM/TSP patients. PBMCs from HAM/TSP patients (n = 5) were FACS sorted, transfected with either Luc or Tax siRNA, and incubated for 24 hours. (**E** and **F**) Tax expression correlated with T-bet expression and IFN-γ production in CD4⁺CCR4⁺ T cells from HAM/TSP patients. CD4⁺CCR4⁺ T cells isolated from HDs and HAM/TSP patients (n = 4 per group) were cultured before being stained for Tax and T-bet protein and analyzed using FACS. IFN-γ production in the culture medium was measured using a CBA assay. ND, not detectable. All data are mean ± SD. P values were calculated using (**A** and **C**) 1-way ANOVA followed by Dunnett test for multiple comparisons, (**B**) Mann-Whitney U test, (**D**) paired t test, or (**E** and **F**) Friedman test followed by Dunn test for multiple comparisons. *$P < 0.05$, ***$P < 0.001$ vs. time point 0.

JPX-9 cell line possessing a stably integrated $CdCl_2$-inducible *Tax* construct and measuring *IFNG* mRNA expression. Inducing *Tax* expression with $CdCl_2$ periodically over 2 weeks yielded a steady rise in *IFNG* expression (Figure 2A). Although there was clearly a correlation between Tax and IFN-γ expression, the *IFNG* expression level was not proportional to that of *Tax*, and the steepest rise in the former was delayed several days after the steepest rise in the latter. Thus, we suspected that expression of 1 or more additional genes may represent an important middle step on the pathway linking Tax and IFN-γ production. DNA microarray results revealed that expression of *TBX21*, which is known to be associated with IFN-γ production, was elevated in CD4⁺CD25⁺CCR4⁺ cells from the HAM/TSP patient, but not the ATLL patient, compared with the HD (Supplemental Figure 1; supplemental material available online with this article; doi:10.1172/JCI75250DS1). *TBX21* mRNA expression, measured via real-time RT-PCR, was elevated in CD4⁺CD25⁺CCR4⁺ cells, but not CD4⁺CD25⁻CCR4⁻ cells, from HAM/TSP patients compared with HDs (Figure 2B). A direct correlation between *Tax* and *TBX21* mRNA expression was then established using the JPX-9 cell line, as described above (Figure 2C). Silencing the *Tax* gene with siRNA in CD4⁺CD25⁺CCR4⁺ cells from HAM/TSP patients reduced *TBX21* as well as *Tax* expression (Figure 2D). Similarly,

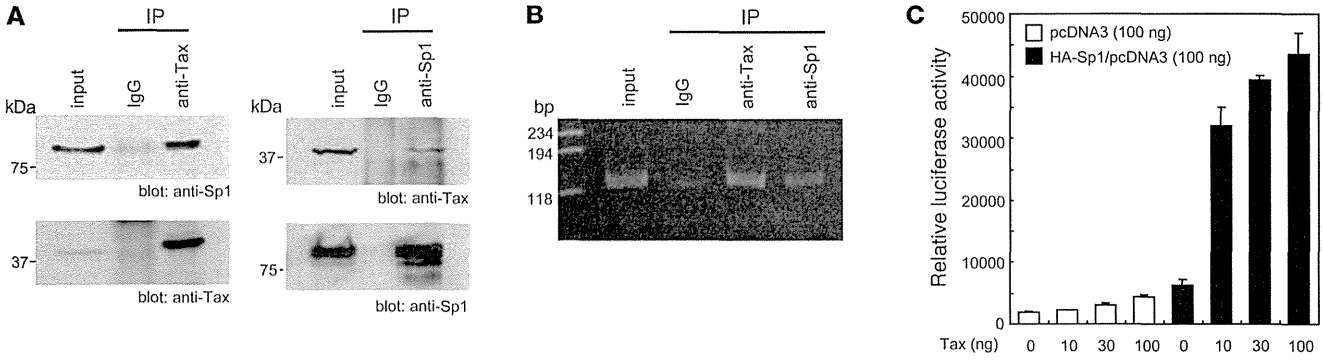

Figure 3. Tax and Sp1 cooperatively enhance *TBX21* promoter activity. (**A**) Co-IP of endogenous Tax and Sp1. Nuclear extracts from MT-2 cells were immunoprecipitated with anti-Tax or anti-Sp1 antibodies or with normal IgG as a control, then immunoblotted with anti-Tax or anti-Sp1 antibodies as indicated. (**B**) Tax bound to the *TBX21* promoter in vivo. ChIP assay using anti-Tax antibody followed by primers encompassing the *TBX21* promoter region (-179 to -59) was performed on genomic DNA isolated from MT-2 cells. DNA (input) and IP with anti-Sp1 served as positive controls, and normal IgG served as a negative control. (**C**) Coactivation of *TBX21* promoter by Sp1 and Tax. HEK293 cells were transfected with 100 ng of *TBX21*-Luc reporter plasmid or Sp1 expression plasmid, as well as 0–100 ng of Tax expression plasmid as indicated. Values were normalized to β-galactosidase activity as an internal control. Data are mean ± SD.

elevation of *Tax* expression via transduction of a GFP-Tax construct into $CD4^+CD25^+CCR4^+$ cells from a HD increased expression of *TBX21* as well as *Tax* (Supplemental Figure 2). Thus, a functional relationship between *Tax* and *TBX21* was confirmed. Finally, among $CD4^+CCR4^+$ cells from HAM/TSP patients, the appearance of Tax^+ cells was associated with a rise in the percentage of $T\text{-}bet^+$ cells, which was associated with a delayed but roughly proportional rise in the amount of IFN-γ protein (Figure 2, E and F). The production of Tax versus T-bet in these $CD4^+CCR4^+$ cells from HAM/TSP patients was compared at 0 versus 48 hours of culturing. At 0 hours, the overwhelming majority of the $CD4^+CCR4^+$ cells were both Tax^- and $T\text{-}bet^-$; by 48 hours, a substantial presence of $Tax^+T\text{-}bet^+$ cells had emerged, and there were very few $T\text{-}bet^+$ cells that were not also Tax^+ (Supplemental Figure 3).

Tax in concert with Sp1 induces TBX21 transcription. Experiments were conducted to investigate the mechanism by which Tax may be involved in *TBX21* transcription in HTLV-1–infected T cells. First, co-IP reactions were performed using nuclear extracts from the HTLV-1–infected MT-2 T cell line to confirm a suspected interaction between endogenous Tax and Sp1, which is known to both form a complex with Tax and to activate *TBX21* transcription (24, 25). Precipitation with anti-Tax or anti-Sp1 antibodies yielded bands corresponding to both Tax and Sp1, whereas precipitation with the nonspecific IgG antibody as the negative control yielded neither band (Figure 3A), thus demonstrating the existence of a Tax-Sp1 complex in HTLV-1–infected T cells. Second, a ChIP assay using primers encompassing the *TBX21* promoter region (-179 to -59) was performed on the MT-2 cells to confirm the suspected interaction between this Tax-Sp1 complex and the *TBX21* promoter. Precipitation with anti-Tax or anti-Sp1, but not IgG, yielded a PCR product corresponding to the *TBX21* promoter (Figure 3B), which suggests that a Tax-Sp1 complex does bind to the *TBX21* promoter site. Finally, a reporter assay was performed using cells transfected with *TBX21*-Luc, a luciferase reporter plasmid containing the *TBX21* promoter region, to confirm a functional relationship among Tax, Sp1, and *TBX21* transcription. Cotransfection with Sp1 resulted in elevated luciferase activity compared with transfection with the reporter alone, and addition of Tax heightened this effect in a concentration-dependent manner (Figure 3C). These findings suggested that Tax, in concert with Sp1, induces *TBX21* transcription.

HTLV-1–infected Th1-like $CCR4^+$ cells are in the CNS of HAM/TSP patients. We next sought to confirm that HTLV-1–infected $CCR4^+$ T cells infiltrate the spinal cords of HAM/TSP patients and exhibit Th1-like traits, such as T-bet and IFN-γ production. Fluorescent immunohistochemical staining of tissue sections from HAM/TSP patient spinal cord lesions revealed the presence of abundant $CCR4^+$ cells infiltrating around the small blood vessels and coexpressing T-bet and IFN-γ (Figure 4A and Supplemental Figure 4). Further investigation revealed that these $CCR4^+$ cells also expressed CXCR3, the marker for Th1 cells (6). It should be noted that both IFN-γ and CXCR3 expression are reported to be induced by T-bet expression (6). Immunofluorescent staining was also used to demonstrate the existence of HTLV-1–infected $CCR4^+$ cells in the CSF of HAM/TSP patients (Figure 4B). $CCR4^+CXCR3^+$ cells were numerous among cells isolated from the CSF of HAM/TSP patients, representing 73.90% of $CD4^+$ cells isolated from a representative patient (Figure 4C) and 63.63% ± 6.73% of $CD4^+$ cells isolated from all patients ($n = 8$; Figure 4D). However, nearly all of these $CD4^+CCR4^+CXCR3^+$ cells were negative for Ki67, a marker of cell proliferation, in the CSF of the HAM/TSP patients (93.94% ± 2.07%, $n = 3$; Figure 4E). The majority of these $CD4^+CCR4^+CXCR3^+$ cells were also $CD25^+$ (70.16% ± 14.08%, $n = 3$, Supplemental Figure 5), confirming the existence of a substantial $CD4^+CD25^+CCR4^+CXCR3^+$ cell population in the CSF of HAM/TSP patients. Importantly, $CD4^+CCR4^+CXCR3^+$ cells did not make up the majority of PBMCs in HAM/TSP patients nor in HDs; in fact, such cells were very few (HAM/TSP, 3.65% ± 1.96%, $n = 8$; HD, 6.88% ± 3.09%, $n = 4$; Figure 4D). PBMCs were also isolated from ATLL patients for comparison, and $CD4^+CCR4^+CXCR3^-$ cells made up the overwhelming majority (83.03% ± 18.61%, $n = 5$; Supplemental Figure 6).

CCR4 shows potential as a molecular target for HAM/TSP immunotherapy. Analysis of HTLV-1 proviral DNA load in subpopulations of $CD4^+$ PBMCs from HAM/TSP patients confirmed that $CCR4^+$ cells were heavily infected, compared with less than

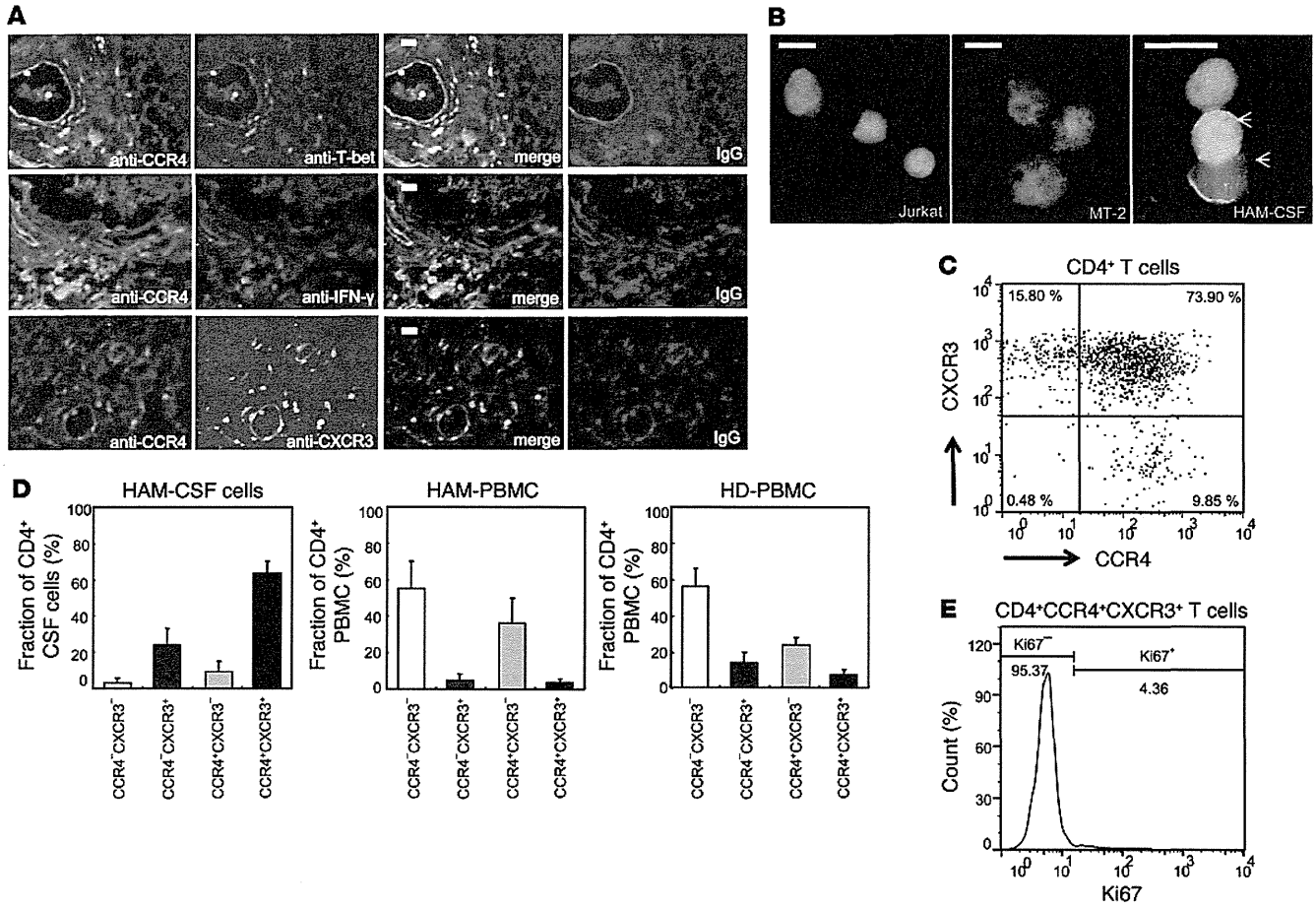

Figure 4. HTLV-1–infected Th1-like CCR4⁺ cells invade the CNS of HAM/TSP patients. (**A**) Detection of CCR4⁺ cells expressing T-bet, IFN-γ, and CXCR3 infiltrating the spinal cord of a HAM/TSP patient. Representative images show immunofluorescent codetection of CCR4 with T-bet, IFN-γ, and CXCR3, as well as the merged images, in thoracic spinal cord sections. Rabbit and goat IgG antibody served as a negative control. Scale bars: 20 μm. (**B**) Presence of HTLV-1–infected CCR4⁺ cells in HAM/TSP patient CSF. Representative images show immunofluorescence-FISH codetection of CCR4 (green) and HTLV-1 provirus (red) in Jurkat cells (uninfected control), MT-2 cells (infected control), and CSF cells from the patients. Arrows denote red provirus signal in the CSF sample. Scale bars: 20 μm. (**C**) CD4⁺ T cells in HAM/TSP patient CSF were mostly CCR4⁺CXCR3⁺. A dot plot of CCR4 and CXCR3 expression in CD4⁺ gated cells isolated from the CSF of a representative HAM/TSP patient is shown. (**D**) CD4⁺CCR4⁺CXCR3⁺ cells were numerous in CSF, but not elevated in peripheral blood, of HAM/TSP patients. Graphs show the percentages of $CCR4^-CXCR3^-$, $CCR4^-CXCR3^+$, $CCR4^+CXCR3^-$ and $CCR4^+CXCR3^+$ T cells among CD4⁺ PBMCs and CSF cells from HAM/TSP patients ($n = 8$) and PBMCs from HDs ($n = 4$). Analysis was performed using FACS. Data are mean ± SD. (**E**) Proliferation was not observed in CD4⁺CCR4⁺CXCR3⁺ cells from HAM/TSP patient CSF. The rate of Ki67 expression, a marker for cell proliferation, is shown for CD4⁺CCR4⁺CXCR3⁺ gated cells from the CSF of a representative HAM/TSP patient.

1% of $CCR4^-$ cells ($n = 7$; Figure 5A). To predict the efficacy of a CCR4⁺ cell–targeting cytotoxic antibody as a treatment for HAM/TSP, PBMCs were isolated from patients ($n = 9$) and analyzed after being cultured with and without the defucosylated chimeric anti-CCR4 monoclonal antibody KM2760 (21) or, for comparison, the steroid therapy prednisolone (PSL). Addition of 1 μg/ml KM2760 significantly reduced the percentage of CCR4⁺ cells, as measured after 7 days ($P = 0.0039$; Figure 5B). As little as 0.1 μg/ml KM2760 was necessary to reduce the HTLV-1 DNA load ($P < 0.05$), whereas PSL had no significant impact (Figure 5C). Use of 1 μg/ml of either KM2760 or PSL was sufficient to suppress spontaneous proliferation of the PBMCs, as measured by ^{3}H-thymidine incorporation ($P < 0.05$ and $P < 0.01$, respectively; Figure 5D) as well as IFN-γ production ($P < 0.05$ and $P < 0.001$, respectively; Figure 5E). Similar results were observed in experiments using cells isolated from the CSF of HAM/TSP patients ($n = 8$): cultures to which 1 μg/ml of KM2760 had been added exhibited reduced HTLV-1 DNA load ($P = 0.0078$; Figure 5F) and IFN-γ production ($P = 0.0391$; Figure 5G). Certain samples shown in Figure 5G did not exhibit this reduction in IFN-γ production; those samples had particularly low cell counts (0.33–2.00 cells/μl), yielding less reliable data. Despite the presence of those lower-quality samples, statistical significance was still established for the sample group as a whole.

Discussion

Previously, we hypothesized that HTLV-1 gives rise to HAM/TSP by altering the behavior of infected cells via Tax expression to yield a new population of Th1-like proinflammatory cells (26). Evidence indicated that a significant portion of this population might be Tregs, as suggested by the CD4⁺CD25⁺CCR4⁺ expres-

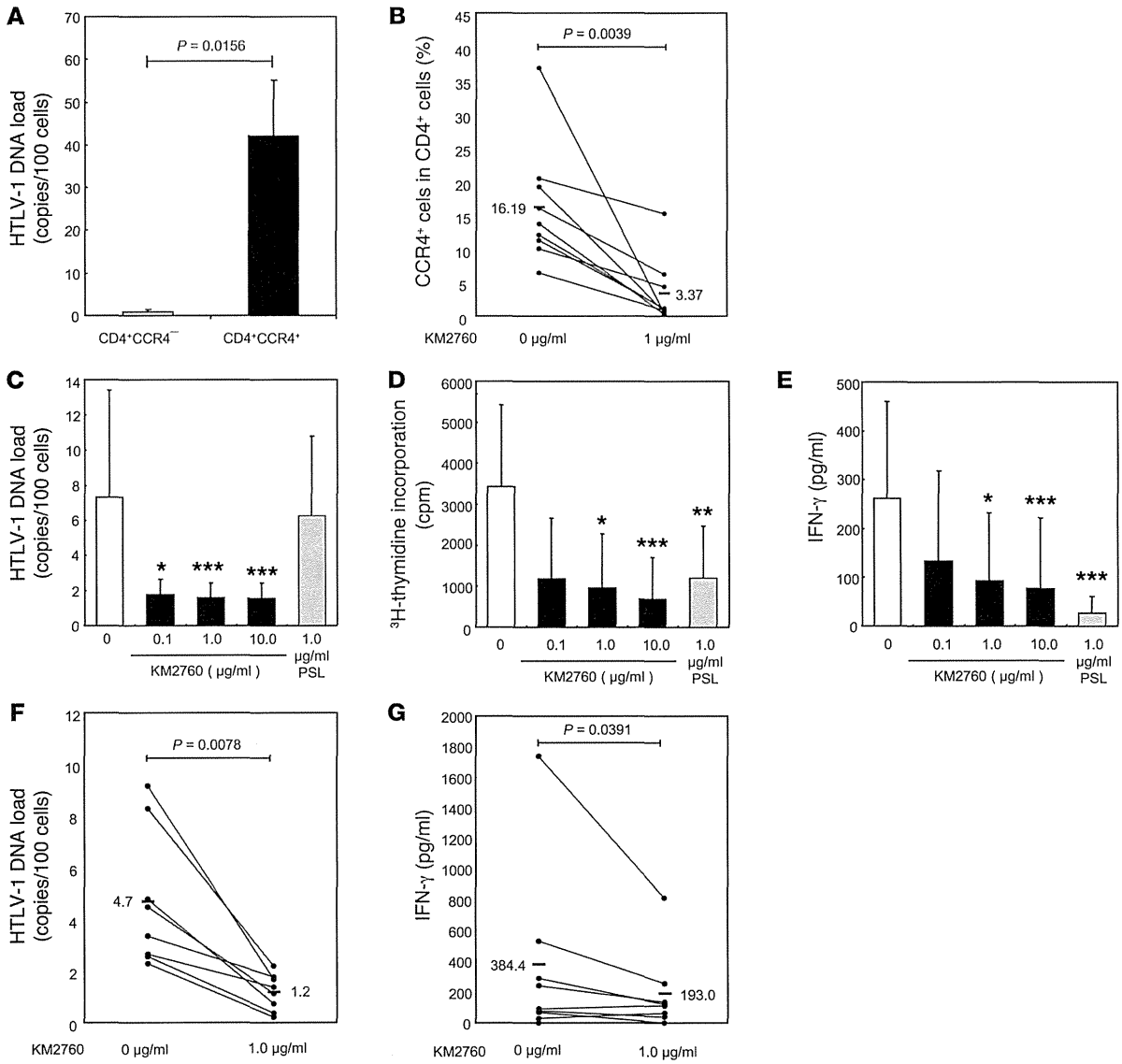

Figure 5. CCR4 shows potential as a molecular target for HAM/TSP immunotherapy. (**A**–**G**) Cells isolated from HAM/TSP patients were sorted via FACS (**A**; $n = 7$) or cultured for 7 days under the following conditions: PBMCs were cultured with various concentrations of KM2760 or 1 μg/ml PSL (**B**–**E**; $n = 9$), and CSF cells were cultured with 1 μg/ml KM2760 (**F** and **G**; $n = 8$). (**A**, **C**, and **F**) HTLV-1 proviral DNA loads were measured using quantitative PCR. (**D**) Degree of spontaneous proliferation was assessed by measuring ^{3}H-thymidine incorporation. (**E** and **G**) IFN-γ production in the culture media was evaluated using CBA assays. HTLV-1 resided in $CD4^+CCR4^+$ rather than $CCR4^-$ cells among PBMCs (**A**), and KM2760 treatment effectively targeted these cells (**B**). Consequently, KM2760 treatment successfully reduced HTLV-1 proviral DNA load (**C**), suppressed spontaneous proliferation (**D**), and decreased IFN-γ production (**E**) in PBMC cultures as well as reducing HTLV-1 DNA load (**F**) and IFN-γ production (**G**) in CSF cell cultures derived from HAM/TSP patients. (**A** and **C**–**E**) Data are mean ± SD. (**B**, **F**, and **G**) Thick horizontal bars represent mean value for all patients; line segments represent individual patients. Statistical analyses were performed using Friedman test followed by Dunn test for multiple comparisons (**C**–**E**) or Wilcoxon test (**A**, **B**, **F**, and **G**). $^*P < 0.05$, $^{**}P < 0.01$, $^{***}P < 0.001$ vs. untreated control.

sion profile (19). We suspected that these infected cells may infiltrate the CNS and trigger an inflammatory positive feedback loop, ultimately leading to chronic spinal cord inflammation (27). In the present study, we provided concrete evidence to support these theories on HAM/TSP pathogenesis, with a particular emphasis on the mechanism by which Tax can induce a proinflammatory phenotype intracellularly via transcriptional regulation.

There is strong evidence to support the conclusion that a substantial portion of the Treg population in HAM/TSP patients is infected with HTLV-1 (28, 29). In a previous study, we demonstrated that $CD4^+CD25^+CCR4^+$ cells were the main reservoir for HTLV-1 in HAM/TSP patients (19), but that expression profile is not exclusive to Tregs. Our present observation that $CD4^+$ T cells positive for FOXP3, a well-established marker for Tregs (10), were more thoroughly infected than the $GATA3^+$ subgroup (Figure 1A) strengthens the argument that Tregs may be the main viral reservoir. It remains debatable whether the virus preferentially infects these cells, promotes their survival (30), or even induces the expression of these

markers. One report postulates that HTLV-1 preferentially infects $CCR4^+$ cells by upregulating CCL22 to encourage cell-to-cell transfer via chemotactic attraction (31). More research is necessary to determine the true mechanism by which infected $CCR4^+$ and $FOXP3^+$ cells become so abundant in HAM/TSP patients.

We demonstrated that the suppressive ability of $CD4^+CD25^+CCR4^+$ cells that characterizes Treg function was impaired by expression of the Tax protein, encoded in the pX region of the HTLV-1 genome (Figure 1B). Prior evidence indicates that Tax may exert these effects via downregulation of FOXP3 expression (20, 32). Transgenic mice expressing Tax exhibit reduced $CD4^+CD25^+FOXP3^+$ Tregs (33) and develop arthritis (34), and transgenic rats expressing HTLV-1 env-pX develop destructive arthropathies, Sjogren syndrome, vasculitis, and polymyositis (35). Collectively, these observations suggest that Tax expression can lead to inflammatory disease by weakening immune tolerance and disrupting homeostasis.

It has long been suspected that in addition to reducing FOXP3 expression, Tax may have the ability to induce IFN-γ production, thereby converting once-suppressive cells into proinflammatory cells. Indeed, intracellular Tax expression has been associated with the rapid upregulation of IFN-γ in infected cells, and researchers have theorized that this upregulation may contribute to the pathogenesis of HTLV-1–associated inflammatory disorders, including HAM/TSP (19, 36, 37). Here we showed at the mRNA level that *Tax* expression stimulated *IFNG* expression; moreover, the effect appeared delayed (Figure 2A), in a manner suggestive of 1 or more intermediate steps in the pathway, rather than direct transcriptional activation. Several candidate pathways have been proposed— such as via NF-κB, STAT1, or STAT5 — but none have been confirmed experimentally (38, 39).

We provided convincing evidence that Tax induces IFN-γ production in infected cells indirectly by amplifying the effects of Sp1 binding to — and increasing the activity of — the *TBX21* promoter: the resulting amplification of T-bet expression was responsible for the rise in IFN-γ production.

T-bet is said to be a Th1-specific T box transcription factor that controls the expression of the hallmark Th1 cytokine, IFN-γ (6). *TBX21*-deficient mice exhibit greater resistance to a variety of inflammatory and autoimmune diseases than their wild-type counterparts (40). Thus, it has been of interest that elevated *TBX21* levels have been found in the PBMCs of HAM/TSP patients (41). We showed that *TBX21* expression was elevated in the $CD4^+CD25^+CCR4^+$ cells of HAM/TSP patients, but not ATLL patients (Figure 2B and Supplemental Figure 1), which suggests that this trait is specific to HAM/TSP pathogenesis. Furthermore, we interpreted the lack of elevation in $CD4^+CD25^-CCR4^-$ cells to indicate that elevated *TBX21* is characteristic of infected cells. Importantly, we clearly demonstrated for the first time that Tax induced T-bet expression (Figure 2, C and E, and Supplemental Figures 2 and 3). Moreover, we showed that this pathway was active in $CD4^+CD25^+CCR4^+$ cells of HAM/TSP patients by silencing Tax expression and observed a corresponding reduction in *TBX21* expression; in the reverse scenario, inducing Tax expression in otherwise-normal $CD4^+CD25^+CCR4^+$ cells from HDs resulted in heightened *TBX21* expression (Figure 2D and Supplemental Figure 2). Finally, we confirmed that this correlation extended to protein production and clearly showed how Tax induces T-bet and subsequently IFN-γ production over time in culture (Figure 2E).

Tax has been reported to stably bind Sp1, a known positive transcriptional regulator of *TBX21* (25, 42). More specifically, interaction with Tax is thought to increase the DNA binding activity of Sp1 (42). Here we used co-IP with samples from the HTLV-1–infected MT-2 cell line to show that endogenous Tax interacted with Sp1 (Figure 3A). Subsequently, ChIP assays revealed that both Sp1 and Tax associated with the *TBX21* promoter region (Figure 3B), a novel finding that supports our theory that Tax and Sp1 together activate *TBX21* transcription. Finally, we showed that in the absence of Sp1, Tax had no significant effect on *TBX21* expression; however, in the presence of Sp1, Tax induced *TBX21* expression in a concentration-dependent manner (Figure 3C). This finding further substantiates our claim that Tax does not directly bind the promoter, but rather acts via Sp1. It should be noted that Tax may induce *TBX21* expression via multiple pathways: it has been reported that Tax enhances STAT1 gene expression in HTLV-1–transformed T cell lines and $CdCl_2$-stimulated JPX-9 cells (38), which suggests that Tax may also induce *TBX21* expression indirectly via STAT1.

The presence of T cell infiltrates in the CNS, indicative of spinal cord inflammation, is a well-known feature of HAM/TSP. Researchers have worked to characterize these cells over the years; together, their findings suggest that the infiltrates are dominated by $CD4^+$ T cells with relatively high proviral loads and elevated Tax and IFN-γ expression (43–45). We hypothesized that a substantial portion of the infiltrate may be made up of infected $CD4^+CCR4^+$ T cells exhibiting Th1-like properties, including IFN-γ production. We used immunohistochemistry to investigate this theory and were able to establish the presence of $CD4^+CCR4^+CXCR3^+$T-$bet^+IFN\text{-}\gamma^+$ cells in spinal cord tissue and HTLV-1–infected $CCR4^+$ cells in the CSF of HAM/TSP patients (Figure 4, A and B). We used FACS analysis to confirm that $CD4^+CCR4^+CXCR3^+$ cells made up the majority of the $CD4^+$ T cells in the HAM/TSP patient CSF (Figure 4C). For the sake of continuity between this and our previous study (19), we also confirmed that the majority of these $CD4^+CCR4^+CXCR3^+$cells were also $CD25^+$ (Supplemental Figure 5), further suggestive of a Treg identity.

We interpret the observation that these $CD4^+CCR4^+CXCR3^+$ cells were virtually nonexistent among PBMCs in HAM/TSP patients (Figure 4D) to mean that the cells had migrated to the CNS, leaving few behind in the periphery. The surprising observation that the Ki67 marker for cell proliferation was negative in the overwhelming majority of $CD4^+CCR4^+CXCR3^+$ cells in the CSF (Figure 4E) signifies that the cells are indeed proliferating elsewhere and subsequently migrating to the CNS. It has in fact been said that HTLV-1–infected cells may be extraordinarily capable of crossing the blood-brain barrier (46). Due to the high proportion of CCR4 positivity among HTLV-1–infected cells (19), the high proviral load in the CSF of HAM/TSP patients (47), and the elevated levels of CCL22 in HAM/TSP patient peripheral blood (30), one might hypothesize that the infected cells migrate across the blood-brain barrier in response to chemokine ligands of CCR4, namely CCL22. However, we found that the CSF of HAM/TSP patients contained only negligible amounts of CCL22, instead favoring the CXCR3 ligand CXCL10 (48). We now postulate that

$CD4^+CCR4^+CXCR3^+$ T cells and other $CXCR3^+$ cells may migrate to the CNS via chemotaxis induced by CXCL10 secreted by astrocytes in the CNS. Previously, we showed that these astrocytes produce CXCL10 in response to IFN-γ, and these levels are further amplified by the invading $CXCR3^+$ cells (27). Together, these findings indicate that a positive feedback loop involving the recruitment of proinflammatory cells to the CNS is the source of chronic inflammation in HAM/TSP, and that the original trigger is the migration of IFN-γ–producing HTLV-1–infected cells to the CNS. Where these proinflammatory cells are primarily proliferating, and why they proliferate at different rates in different settings, are questions to be addressed in future studies.

Our findings in this and previous studies imply that targeting $CCR4^+$ cells could constitute an effective treatment for HAM/TSP. Indeed, this strategy is already in play for ATLL patients, the majority of whom suffer from $CCR4^+$ T cell–derived cancers (7). The humanized defucosylated anti-CCR4 monoclonal antibody KW-0761, which has been shown to induce CCR4-specific ADCC, has been approved as a treatment for ATLL (49, 50). The observation that the majority of infected $CD4^+$ PBMCs in HAM/TSP patients were $CCR4^+$ (Figure 5A) suggests that an anti-CCR4 antibody with ADCC properties might be used to effectively treat HAM/TSP patients as well. Steroids are currently the standard of care for HAM/TSP patients, but this approach is not considered optimal: as with many nonspecific treatments, the effectiveness is limited, and the side effects are numerous (51). Here we compared the effects of the defucosylated chimeric anti-CCR4 monoclonal antibody KM2760 (21) with those of the steroid PSL on ex vivo cultures of cells from HAM/TSP patients. Although PSL had more potent effects per microgram, both treatments successfully reduced cell proliferation and IFN-γ production (Figure 5, D, E, and G). In addition, even a small dose of the antibody effectively reduced proviral load, whereas PSL treatment had no significant effect (Figure 5, C and F). These findings support the main premise of this paper, namely, that $CCR4^+$ cells are major viral reservoirs and producers of IFN-γ. Our study is the first to test the effects of such an antibody-based treatment on cells from HAM/TSP patients; the results were promising, and a clinical trial investigating the in vivo effectiveness in HAM/TSP patients is now underway. Importantly, our research indicates that even if the antibody does not cross the blood-brain barrier, it could be therapeutically effective against spinal cord inflammation by eliminating the proinflammatory $CCR4^+$ cells in the peripheral blood that would have migrated to the CNS.

Until very recently, there had been no reports of T cell character changing from suppressive to inflammatory in response to internal transcriptional alterations induced intracellularly by viral products. There have been many reports of Tregs transforming in the presence of inflammation due to the influence of cytokines, including instances where FOXP3 expression is lost and even cases where IFN-γ production is gained (12, 13). The only report of a similar phenomenon occurring via an intracellular virus-induced pathway states that the HTLV-1 basic leucine zipper (HBZ) gene product can reduce the expression of FOXP3 in HBZ-transgenic mouse Tregs (52). Here we showed for the first time that the HTLV-1 virus can similarly affect gene expression in human cells, inducing IFN-γ production, as well as reduce suppressive function. Collectively, the research to date suggests that HTLV-1 may preferentially infect $CCR4^+$ cells, including Tregs, and induce transcriptional changes via Tax that not only reduce FOXP3 expression, but also induce T-bet expression and consequently IFN-γ production, yielding a proinflammatory immune imbalance. While there is considerable evidence to support this theory, further experiments are necessary to prove that this pathway is indeed the origin of HAM/TSP chronic inflammation. However, here we have directly shown that the HTLV-1 protein product Tax can induce the expression of the Th1 master transcription factor T-bet, which certainly implies that HTLV-1 is capable of activating inherent plasticity in T cells and shifting their gene expression profiles toward a Th1-like state.

Methods

Patient selection and sample preparation. The study included HTLV-1–noninfected HDs ($n = 8$, 4 male and 4 female; mean age, 36 yr), asymptomatic carriers ($n = 6$, 4 male and 2 female; mean age, 56 yr), ATLL patients ($n = 6$, 2 male and 4 female; mean age, 68 yr), and HAM/TSP patients ($n = 31$, 9 male and 22 female; mean age, 61 yr). Diagnosis of ATLL was based on the criteria established by Shimoyama (53). HTLV-1 seropositivity was determined by a particle agglutination assay (Serodia-HTLV-1) and confirmed by Western blot (SRL Inc.). HAM/TSP was diagnosed according to WHO guidelines (54).

Samples of PBMCs were prepared using density gradient centrifugation (Pancoll; PAN-Biotech) and viably cryopreserved in liquid nitrogen (Cell Banker 1; Mitsubishi Chemical Medience Corp.). CSF samples were taken from 17 HAM/TSP patients. CSF cells were isolated by centrifugation and cryopreserved in the aforementioned freezing medium until use. Thoracic spinal cord tissue samples from 1 HAM/TSP patient were obtained postmortem, fixed in 10% formalin, and embedded in paraffin.

Antibodies. For FACS studies, labeled anti-CD3 (UCHT1), anti-CD4 (OKT4), anti-GATA3 (TWAJ), and anti-FOXP3 (PCH101) were purchased from eBioscience, and labeled anti-CCR4 (1G1), anti-CD25 (BC96), anti-CXCR3 (1C6), anti–T-bet (4B10), and anti-Ki67 (B56) were purchased from BD Biosciences. For IP studies, anti-Sp1 (PEP2) and normal IgG were purchased from Santa Cruz Biotechnology Inc., and anti-Tax (Lt-4) was prepared as described previously (55). For immunofluorescence studies, anti-CCR4, anti–IFN-γ, and anti-CXCR3 were purchased from Abcam; anti–T-bet was purchased from Santa Cruz Biotechnology Inc.; and Alexa Fluor 488– and Alexa Fluor 594–conjugated secondary antibodies were purchased from Invitrogen. Kyowa Hakko Kirin Co. Ltd. provided KM2760, a chimeric anti-CCR4 IgG1 monoclonal antibody (21).

Plasmids. The *TBX21*-Luc reporter gene plasmid was constructed as described previously (25). The 100-bp promoter fragment (–101 to –1) in the 5′-flanking region of the human *TBX21* gene was obtained by PCR using human PBMC genomic DNA as the template. Primers used for PCR were 5′-CGCCTCGAGGGCGGGGTGGGGCGAGGCGG-3′ and 5′-CCCAAGCTTCTGTCACTAGAGTCGCAGCGCTTT-3′. The amplified PCR product was digested with XhoI/HindIII and cloned into pPicaGene-Basic vector II (Toyo-ink), which yielded *TBX21*-Luc. Creation of the human Sp1 construct with HA-tag added to the N terminus was accomplished via real-time RT-PCR amplification of human PBMC cDNA with the following primers: Sp1 forward, 5′-CGCGAATTCATGAGCGACCAAGATCACTCCATGGA-3′; Sp1 reverse, 5′-CGCCTCGAGTCAGAAGCCATTGCCACTGATATTAATGGAC-3′. The amplified fragment was digested with EcoRI/XhoI and

subcloned into HA-tagged pcDNA3 (Invitrogen). Tax construct with FLAG-tag added to the N terminus was prepared via PCR amplification of template DNA (56) with the following primers: Tax forward, 5′-CGCGAATTCATGGCCCACTTCCCAGGGTTT-3′; Tax reverse, 5′-CGCCTCGAGTCAGACTTCTGTTTCACGGAAATGTTTTTC-3′. The amplified fragment was digested with EcoRI/XhoI and subcloned into FLAG-tagged pcDNA3. The plasmid HTLV-1 provirus (pUC/HTLV-1) was provided by T. Watanabe (University of Tokyo, Tokyo, Japan) (57). A lentiviral vector, CSIICMV, was used as a null expression vector for lentiviral infection (provided by H. Miyoshi, RIKEN BioResource Center, Tsukuba, Japan) (58). CSIICMV/GFP and CSIICMV/GFP-Tax, which express GFP and GFP fused Tax, were constructed by inserting digested GFP and GFP-Tax from pEGFP (Clontech) and pEGFP-Tax, respectively, into CSIICMV.

Flow cytometric analysis. PBMCs and CSF cells were immunostained with various combinations of the following fluorescence-conjugated antibodies that tag cell surface markers: CD3 (UCHT1), CD4 (OKT4), CD25 (BC96), CCR4 (1G1), CXCR3 (1C6). In some experiments, cells were fixed with a staining buffer set (eBioscience), then intracellularly stained with antibodies against T-bet (4B10), FOXP3 (PCH101), and GATA3 (TWAJ). Cells were stained with a saturating concentration of antibody in the dark (4°C, 30 minutes) and washed twice before analysis using FACSCalibur or LSR II (BD Biosciences). Data were processed using FlowJo software (TreeStar). For cell sorting, JSAN (Bay Bioscience) was used, and the purity exceeded 95%.

Cell isolation. $CD4^+CD25^+CCR4^+$ cells, $CD4^+CD25^-CCR4^-$ cells, $CD4^+GATA3^+$ cells, and $CD4^+FOXP3^+$ cells were separated by FACS sorting. $CD4^+$ T cells were isolated from PBMCs using negative selection with magnetic beads (MACS $CD4^+$ T cell isolation kit; Miltenyi Biotec). $CD4^+CCR4^-$ or $CD4^+CCR4^+$ cells were then isolated from these $CD4^+$ T cells using positive selection with anti-CCR4 Ab (1G1) and rat anti-mouse IgG1 microbeads (Miltenyi Biotec).

Cell culture conditions. HEK293 cells were cultured in MEM (Wako Pure Chemical Industries) supplemented with 10% heat-inactivated FBS (Gibco, Invitrogen) and 1% penicillin/streptomycin (P/S) (Wako Pure Chemical Industries). HEK293T cells were cultured in DMEM-high glucose (Sigma-Aldrich) supplemented with 10% FBS and 1% P/S. Jurkat, MT-2, and JPX-9 cells were cultured in RPMI 1640 medium (Wako Pure Chemical Industries) supplemented with 10% FBS and 1% P/S. JPX-9 is a subline of Jurkat carrying Tax under the control of the metallothionein promoter (provided by M. Nakamura, Tokyo Medical and Dental University, Tokyo, Japan) (59), by which Tax expression is inducible by the addition of 20 μM $CdCl_2$ (Nacalai Tesque Inc.). PBMCs, $CD4^+CCR4^+$ cells, $CD4^+CD25^+CCR4^+$ cells, and $CD4^+CD25^-CCR4^-$ cells isolated from HDs or HAM/TSP patients were cultured in RPMI 1640 medium supplemented with 5% human AB serum (Gibco, Invitrogen) and 1% P/S.

Gene expression profiling and analyses. For transcriptional profiling, $CD4^+CD25^+CCR4^+$ T cells from a HAM/TSP patient, an ATLL patient, and an HD were separated using FACS sorting. Total RNA was prepared using ISOGEN (Nippon gene) following the manufacturer's recommendations. RNA was amplified and labeled with cyanine 3 (Cy3) using an Agilent Quick Amp Labeling Kit, 1-color (Agilent Technologies), following the manufacturer's instructions. For each hybridization, Cy3-labeled cRNA were fragmented and hybridized to an Agilent Human GE 4x44K Microarray (design ID 014850). After washing, microarrays were scanned using an Agilent DNA microarray scanner. Intensity values of each scanned feature were quantified using Agilent feature extraction software (version 9.5.3.1), which performs background subtractions. All data were analyzed using GeneSpring GX software (Agilent Technologies). There were a total of 41,000 probes on Agilent Human GE 4x44K Microarray (design ID 014850), not including control probes. Microarray data were deposited in GEO (accession no. GSE57259).

Real-time PCR and real-time RT-PCR. The HTLV-1 proviral DNA load was measured using ABI Prism 7500 SDS (Applied Biosystems) as described previously (19). For real-time RT-PCR analysis, total RNA isolation and cDNA synthesis were performed as described previously (19). Real-time PCR reactions were carried out using TaqMan Universal Master Mix (Applied Biosystems) and Universal Probe Library assays designed using ProbeFinder software (Roche Applied Science). ABI Prism 7500 SDS was programmed to have an initial step of 2 minutes at 50°C and 10 minutes at 95°C, followed by 45 cycles of 15 seconds at 95°C and 1 minute at 60°C. The primers used were as follows: *TBX21*, 5′-TGTGGTCCAAGTTTAATCAGCA-3′ (forward) and 5′-TGACAGGAATGGGAACATCC-3′ (reverse) (probe no. 9; Roche Applied Science); *Tax*, 5′-ATACAACCCCCAACATTCCA-3′ (forward) and 5′-TTTCGGAAGGGGGAGTATTT-3′ (reverse) (probe no. 69; Roche Applied Science). The primers and probes for detecting *Tax*, *IFNG*, and *GAPDH* mRNA were described previously (19). Relative quantification of mRNA was performed using the comparative Ct method using GAPDH as an endogenous control. For each sample, target gene expression was normalized to the expression of GAPDH, calculated as $2^{-(Ct[target] - Ct[GAPDH])}$.

Virus preparation and cell infection. 293T cells (1×10^6) plated in 100-mm dishes were cotransfected with the appropriate lentiviral-GFP or lentiviral-GFP-Tax expression vector (17 μg), vesicular stomatitis virus G expression vector VSV-G (pMD.G) (5 μg), rev expression vector pRSVRev (5 μg), and gag-pol expression vector pMDLg/pRRE (12 μg) (60) using Lipofectamine 2000 (Invitrogen) according to the manufacturer's protocol. After 4 hours, cells were washed 3 times with PBS, 5 ml of new medium was added, and cells were incubated for 48 hours. Culture supernatants were harvested and filtered through 0.45-μm pore size filters. Lentivirus was concentrated approximately 40-fold by low centrifugation at 6,000 *g* for 16 hours and resuspended in 2 ml RPMI 1640 medium. Freshly isolated $CD4^+CD25^+CCR4^+$ T cells were activated using Treg Suppression Inspector (Anti-Biotin MACSiBead Particles preloaded with biotinylated CD2, CD3, and CD28 antibodies) according to the manufacturer's protocol (Miltenyi Biotec). After being cultured for 36 hours, cells were transduced with equal amounts of the GFP or GFP-Tax lentivirus (MOI 15), followed by centrifugation for 1 hour at 780 *g*, 32°C. After being cultured for 4 hours at 32°C, cells were washed with culture medium and cultured in round-bottomed 96-well plates at 37°C.

Treg suppression assay. A study was conducted to compare the capacities of GFP versus GFP-Tax lentivirus–infected $CD4^+CD25^+CCR4^+$ T cells to suppress cell proliferation. T cell samples were taken from HDs, and 5×10^4 $CD4^+CD25^-$ T cells were stimulated with the Treg Suppression Inspector (see above) according to the manufacturer's instructions. These cells were then cocultured with 5×10^4 GFP lentivirus–infected $CD4^+CD25^+CCR4^+$ T cells or GFP-Tax lentivirus–infected $CD4^+CD25^+CCR4^+$ T cells. After culturing for 4 days, cell proliferation was measured using a ^{3}H-thymidine incorporation assay as described previously (19).

RNA interference assay. siRNA was synthesized chemically at Hokkaido System Science. The sequences of siRNA oligonucleotides were as follows: Tax, 5′-GGCCUUAUUUGGACAUUUATT-3′ and 5′-UAAAUGUCCAAAUAAGGCCTT-3′ (31); Luc, 5′-CGUACGCG-GAAUACUUCGATT-3′ and 5′-UCGAAGUAUUCCGCGUACGTT3′. Next, 100 pmol annealed RNA duplex was transfected using Human T cell Amaxa Nucleofector Kit according to the manufacturer's recommendations (Lonza). 100 pmol Luc siRNA was used as a negative control. Cells were incubated for 48 hours and then harvested and subjected to real-time RT-PCR analysis.

Measurement of IFN-γ. IFN-γ concentration in the culture supernatant was measured with a cytometric bead array kit (BD Biosciences) using a FACSCalibur flow cytometer (BD Biosciences) according to the manufacturer's instructions.

IP. Approximately 1 mg of MT-2 nuclear extracts were incubated with 5 μg anti-Tax, anti-Sp1, or normal IgG coupled with protein G–agarose (Roche Applied Science) in IP buffer (10 mM HEPES [pH 7.9], 100 mM KCl, 1 mM EDTA, 1 mM dithiothreitol, 0.1% NP-40, 1 mM Na_3VO_4, 5 mM NaF, 2 μg/ml aprotinin, 2 μg/ml leupeptin, and 2 μg/ml pepstatin) for 2 hours. The precipitated proteins were washed with the IP buffer, separated by 10% SDS-PAGE, and immunoblotted with anti-Tax or anti-Sp1 antibodies.

ChIP assay. ChIP assay was performed using a ChIP assay kit (Upstate Biotechnology) with some modifications. Briefly, 5×10^6 MT-2 cells were fixed with 1% formaldehyde at 37°C for 25 minutes and washed twice with PBS. Cells were subsequently harvested and sonicated in lysis buffer. Precleared chromatin samples were immunoprecipitated with 5 μg anti-Tax antibody, anti-Sp1 antibody, or normal IgG for 16 hours at 4°C. Immune complexes were collected with salmon sperm DNA/protein G–sepharose for 90 minutes with rotation, washed, and then incubated at 65°C for 6 hours for reverse cross-linking. Chromatin DNA was extracted and analyzed using PCR with primers for the *TBX21* promoter region (–179 to –59; forward, 5′-GCCAAGAGCGTAGAATTTGC-3′; reverse, 5′-CGCTTT-GCTGTGGCTTTATG-3′) (25, 61). Amplification was performed using ExTaq (Takara Bio) with 1 cycle at 95°C for 5 minutes followed by 30 cycles of 95°C for 30 seconds, 54°C for 30 seconds, and 72°C for 30 seconds. Amplified products were analyzed using 8% polyacrylamide gel electrophoresis.

Luciferase assay. For transient transfection, HEK293 cells were seeded at 5×10^4 cells/well into 24-well plates. After 12 hours, medium was changed to MEM supplemented with 10% FBS and 1% P/S, and each plasmid was transfected with CellPhect Transfection Kit according to the manufacturer's recommendations (GE Healthcare). 50 ng pRSV-βgal plasmid was included in each transfection experiment to control for the efficiency of transfection. The total amount of transfected DNA was kept constant with pcDNA3 in all samples. After 48 hours, cells were lysed with Passive Lysis Buffer (Promega), and luciferase activity was measured using the Promega luciferase assay system and MicroLumat Plus LB96V (Berthold Technologies). Values were normalized to β-galactosidase activity as an internal control.

Tissue staining. Formalin-fixed thoracic spinal cord tissue sections were deparaffinized in xylene and rehydrated in a series of graded alcohols and distilled water. The antigenicity of the tissue sections was recovered using a standard microwave heating technique. For immunofluorescence, the slides were incubated in PBS with 10% goat serum for 1 hour at room temperature, then in anti-CCR4 antibody, anti–T-bet antibody, anti–IFN-γ antibody, and anti-CXCR3 antibody overnight at 4°C, labeled with Alexa Fluor 488– or Alexa Fluor 594–conjugated secondary antibody, and examined under a fluorescence microscope (Nikon eclipse E600 with fluorescence filter Nikon F-FL; Nikon Instech) with rabbit or goat IgG as the negative control. Tissue sections were also stained with H&E.

Immunofluorescence staining and immunofluorescence-FISH. Jurkat cells, MT-2 cells, and cells from the CSF of 3 HAM/TSP patients were attached to slides using a cytospin centrifuge (Thermo Fisher Scientific) and fixed in 4% paraformaldehyde (Wako Pure Chemical Industries) for 30 minutes. The slides were washed with PBS and then pretreated as follows: slides were immersed in room temperature 0.2M HCl for 20 minutes, followed by 0.2% Triton-X/PBS for 10 minutes, and finally 0.005% pepsin/0.1M HCl heated to 37°C for 5 minutes. After pretreatment, the slides were stained using the immunofluorescence Can Get Signal kit (TOYOBO) according the manufacturer's instructions with anti-CCR4 as the primary antibody and Alexa Fluor 488–conjugated anti-goat IgG as the secondary antibody. After again being fixed with 4% paraformaldehyde, cells were incubated with a nick-translated (Spectrum Red) pUC/HTLV-1 DNA probe, first for 5 minutes at 70°C and then overnight at 37°C. Images were obtained under an automated research microscope (Leica DMRA2) and analyzed with CW4000 FISH software (Leica Microsystems).

Proliferation assay. PBMCs from HAM/TSP patients were plated into 96-well round-bottomed plates (1×10^5 cells/well) and cultured without any mitogenic stimuli. Cell proliferation was measured using a ^3H-thymidine incorporation assay as described previously (19).

Statistics. Paired 2-tailed Student's *t* test and Wilcoxon test were used for within-group comparisons. Unpaired 2-tailed Student's *t* test or Mann-Whitney *U* test was used for between-group comparisons. 1-way ANOVA was used for multiple comparisons, followed by Dunnett or Tukey test. Friedman test was used for paired multiple comparisons, followed by Dunn test. Statistical analyses were performed using Graphpad Prism 5 (GraphPad Software Inc.). A *P* value less than 0.05 was considered significant.

Study approval. Written informed consent was obtained from all patients before the study, which was reviewed and approved by the Institutional Ethics Committee at St. Marianna University and conducted in compliance with the tenets of the Declaration of Helsinki.

Acknowledgments

The authors acknowledge the excellent technical assistance provided by Yumiko Hasegawa, M. Koike, Y. Suzuki-Ishikura, and Y. Saito. This work was partly supported by project "Research on Measures for Intractable Disease"; by a matching fund subsidy from the Ministry of Health Labour and Welfare; by JSPS KAKENHI grant nos. 24790898, 25461294, and 25461293; by the Takeda Science Foundation; and by the Daiichi Sankyo Foundation of Life Science.

Address correspondence to: Yoshihisa Yamano, Department of Rare Diseases Research, Institute of Medical Science, St. Marianna University School of Medicine, 2-16-1 Sugao, Miyamae-ku, Kanagawa 216-8512, Japan. Phone: 81.44.977.8111; E-mail: yyamano@marianna-u.ac.jp.

1. Murphy KM, Stockinger B. Effector T cell plasticity: flexibility in the face of changing circumstances. *Nat Immunol*. 2010;11(8):674–680.
2. Cosmi L, Maggi L, Santarlasci V, Liotta F, Annunziato F. T helper cells plasticity in inflammation. *Cytometry A*. 2014;85(1):36–42.
3. Long SA, Buckner JH. CD4+FOXP3+ T regulatory cells in human autoimmunity: more than a numbers game. *J Immunol*. 2011;187(5):2061–2066.
4. Zhou X, Bailey-Bucktrout S, Jeker LT, Bluestone JA. Plasticity of CD4(+) FoxP3(+) T cells. *Curr Opin Immunol*. 2009;21(3):281–285.
5. Hori S, Nomura T, Sakaguchi S. Control of regulatory T cell development by the transcription factor Foxp3. *Science*. 2003;299(5609):1057–1061.
6. Zhu J, Paul WE. CD4 T cells: fates, functions, and faults. *Blood*. 2008;112(5):1557–1569.
7. Ishida T, Ueda R. Immunopathogenesis of lymphoma: focus on CCR4. *Cancer Sci*. 2011;102(1):44–50.
8. Finney OC, Riley EM, Walther M. Phenotypic analysis of human peripheral blood regulatory T cells (CD4+FOXP3+CD127lo/–) ex vivo and after in vitro restimulation with malaria antigens. *Eur J Immunol*. 2010;40(1):47–60.
9. Mjosberg J, Berg G, Jenmalm MC, Ernerudh J. FOXP3+ regulatory T cells and T helper 1, T helper 2, and T helper 17 cells in human early pregnancy decidua. *Biol Reprod*. 2010;82(4):698–705.
10. Williams LM, Rudensky AY. Maintenance of the Foxp3-dependent developmental program in mature regulatory T cells requires continued expression of Foxp3. *Nat Immunol*. 2007;8(3):277–284.
11. Bennett CL, et al. The immune dysregulation, polyendocrinopathy, enteropathy, X-linked syndrome (IPEX) is caused by mutations of FOXP3. *Nat Genet*. 2001;27(1):20–21.
12. Gao Y, et al. Molecular mechanisms underlying the regulation and functional plasticity of FOXP3(+) regulatory T cells. *Genes Immun*. 2012;13(1):1–13.
13. Dominguez-Villar M, Baecher-Allan CM, Hafler DA. Identification of T helper type 1-like, Foxp3+ regulatory T cells in human autoimmune disease. *Nat Med*. 2011;17(6):673–675.
14. Sakaguchi S, et al. Foxp3+ CD25+ CD4+ natural regulatory T cells in dominant self-tolerance and autoimmune disease. *Immunol Rev*. 2006;212:8–27.
15. Viglietta V, Baecher-Allan C, Weiner HL, Hafler DA. Loss of functional suppression by CD4+CD25+ regulatory T cells in patients with multiple sclerosis. *J Exp Med*. 2004;199(7):971–979.
16. Kanangat S, et al. Disease in the scurfy (sf) mouse is associated with overexpression of cytokine genes. *Eur J Immunol*. 1996;26(1):161–165.
17. Lyon MF, Peters J, Glenister PH, Ball S, Wright E. The scurfy mouse mutant has previously unrecognized hematological abnormalities and resembles Wiskott-Aldrich syndrome. *Proc Natl Acad Sci U S A*. 1990;87(7):2433–2437.
18. Clark LB, Appleby MW, Brunkow ME, Wilkinson JE, Ziegler SF, Ramsdell F. Cellular and molecular characterization of the scurfy mouse mutant. *J Immunol*. 1999;162(5):2546–2554.
19. Yamano Y, et al. Abnormally high levels of virus-infected IFN-γ+ CCR4+ CD4+ CD25+ T cells in a retrovirus-associated neuroinflammatory disorder. *PLoS One*. 2009;4(8):e6517.
20. Yamano Y, et al. Virus-induced dysfunction of CD4+CD25+ T cells in patients with HTLV-I-associated neuroimmunological disease. *J Clin Invest*. 2005;115(5):1361–1368.
21. Niwa R, et al. Defucosylated chimeric anti-CC chemokine receptor 4 IgG1 with enhanced antibody-dependent cellular cytotoxicity shows potent therapeutic activity to T-cell leukemia and lymphoma. *Cancer Res*. 2004;64(6):2127–2133.
22. Yoshida M, Seiki M, Yamaguchi K, Takatsuki K. Monoclonal integration of human T-cell leukemia provirus in all primary tumors of adult T-cell leukemia suggests causative role of human T-cell leukemia virus in the disease. *Proc Natl Acad Sci U S A*. 1984;81(8):2534–2537.
23. Cook LB, Rowan AG, Melamed A, Taylor GP, Bangham CR. HTLV-1-infected T cells contain a single integrated provirus in natural infection. *Blood*. 2012;120(17):3488–3490.
24. Zhang L, Zhi H, Liu M, Kuo YL, Giam CZ. Induction of p21(CIP1/WAF1) expression by human T-lymphotropic virus type 1 Tax requires transcriptional activation and mRNA stabilization. *Retrovirology*. 2009;6:35.
25. Yu J, et al. Transcriptional control of human T-BET expression: the role of Sp1. *Eur J Immunol*. 2007;37(9):2549–2561.
26. Araya N, et al. Human T-lymphotropic virus type 1 (HTLV-1) and regulatory T cells in HTLV-1-associated neuroinflammatory disease. *Viruses*. 2011;3(9):1532–1548.
27. Ando H, et al. Positive feedback loop via astrocytes causes chronic inflammation in virus-associated myelopathy. *Brain*. 2013; 136(pt 9):2876–2887.
28. Kohno T, et al. Possible origin of adult T-cell leukemia/lymphoma cells from human T lymphotropic virus type-1-infected regulatory T cells. *Cancer Sci*. 2005;96(8):527–533.
29. Satou Y, Utsunomiya A, Tanabe J, Nakagawa M, Nosaka K, Matsuoka M. HTLV-1 modulates the frequency and phenotype of FoxP3+CD4+ T cells in virus-infected individuals. *Retrovirology*. 2012;9:46.
30. Toulza F, et al. Human T-lymphotropic virus type 1-induced CC chemokine ligand 22 maintains a high frequency of functional FoxP3+ regulatory T cells. *J Immunol*. 2010;185(1):183–189.
31. Hieshima K, Nagakubo D, Nakayama T, Shirakawa AK, Jin Z, Yoshie O. Tax-inducible production of CC chemokine ligand 22 by human T cell leukemia virus type 1 (HTLV-1)-infected T cells promotes preferential transmission of HTLV-1 to CCR4-expressing CD4+ T cells. *J Immunol*. 2008;180(2):931–939.
32. Grant C, Oh U, Yao K, Yamano Y, Jacobson S. Dysregulation of TGF-β signaling and regulatory and effector T-cell function in virus-induced neuroinflammatory disease. *Blood*. 2008;111(12):5601–5609.
33. Ohsugi T, Kumasaka T. Low CD4/CD8 T-cell ratio associated with inflammatory arthropathy in human T-cell leukemia virus type I Tax transgenic mice. *PLoS One*. 2011;6(4):e18518.
34. Iwakura Y, et al. Induction of inflammatory arthropathy resembling rheumatoid arthritis in mice transgenic for HTLV-I. *Science*. 1991;253(5023):1026–1028.
35. Nakamaru Y, et al. Immunological hyperresponsiveness in HTLV-I LTR-env-pX transgenic rats: a prototype animal model for collagen vascular and HTLV-I-related inflammatory diseases. *Pathobiology*. 2001;69(1):11–18.
36. Hanon E, et al. High production of interferon gamma but not interleukin-2 by human T-lymphotropic virus type I-infected peripheral blood mononuclear cells. *Blood*. 2001;98(3):721–726.
37. Yamazato Y, Miyazato A, Kawakami K, Yara S, Kaneshima H, Saito A. High expression of p40(tax) and pro-inflammatory cytokines and chemokines in the lungs of human T-lymphotropic virus type 1-related bronchopulmonary disorders. *Chest*. 2003;124(6):2283–2292.
38. Nakamura N, et al. Human T-cell leukemia virus type 1 Tax protein induces the expression of STAT1 and STAT5 genes in T-cells. *Oncogene*. 1999;18(17):2667–2675.
39. Sun SC, Yamaoka S. Activation of NF-kappaB by HTLV-I and implications for cell transformation. *Oncogene*. 2005;24(39):5952–5964.
40. Lazarevic V, Glimcher LH. T-bet in disease. *Nat Immunol*. 2011;12(7):597–606.
41. Nishiura Y, Nakamura T, Fukushima N, Moriuchi R, Katamine S, Eguchi K. Increased mRNA expression of Th1-cytokine signaling molecules in patients with HTLV-I-associated myelopathy/tropical spastic paraparesis. *Tohoku J Exp Med*. 2004;204(4):289–298.
42. Trejo SR, Fahl WE, Ratner L. The tax protein of human T-cell leukemia virus type 1 mediates the transactivation of the c-sis/platelet-derived growth factor-B promoter through interactions with the zinc finger transcription factors Sp1 and NGFI-A/Egr-1. *J Biol Chem*. 1997;272(43):27411–27421.
43. Furuya T, et al. Heightened transmigrating activity of CD4-positive T cells through reconstituted basement membrane in patients with human T-lymphotropic virus type I-associated myelopathy. *Proc Assoc Am Physicians*. 1997; 109(3):228–236.
44. Moritoyo T, et al. Detection of human T-lymphotropic virus type I p40tax protein in cerebrospinal fluid cells from patients with human T-lymphotropic virus type I-associated myelopathy/tropical spastic paraparesis. *J Neurovirol*. 1999;5(3):241–248.
45. Umehara F, Izumo S, Ronquillo AT, Matsumuro K, Sato E, Osame M. Cytokine expression in the spinal cord lesions in HTLV-I-associated myelopathy. *J Neuropathol Exp Neurol*. 1994;53(1):72–77.
46. Matsuura E, Yamano Y, Jacobson S. Neuroimmunity of HTLV-I Infection. *J Neuroimmune Pharmacol*. 2010;5(3):310–325.
47. Nagai M, Yamano Y, Brennan MB, Mora CA, Jacobson S. Increased HTLV-I proviral load and preferential expansion of HTLV-I Tax-specific CD8+ T cells in cerebrospinal fluid from patients with HAM/TSP. *Ann Neurol*. 2001;50(6):807–812.
48. Sato T, et al. CSF CXCL10, CXCL9, and neopterin as candidate prognostic biomarkers for HTLV-1-associated myelopathy/tropical spastic paraparesis. *PLoS Negl Trop Dis*. 2013;7(10):e2479.
49. Yamamoto K, et al. Phase I study of KW-0761, a defucosylated humanized anti-CCR4 antibody, in relapsed patients with adult T-cell leukemia-lymphoma and peripheral T-cell lymphoma.

J Clin Oncol. 2010;28(9):1591–1598.
50. Ishida T, et al. Defucosylated anti-CCR4 monoclonal antibody (KW-0761) for relapsed adult T-cell leukemia-lymphoma: a multicenter phase II study. *J Clin Oncol.* 2012;30(8):837–842.
51. Yamano Y, Sato T. Clinical pathophysiology of human T-lymphotropic virus-type 1-associated myelopathy/tropical spastic paraparesis. *Front Microbiol.* 2012;3:389.
52. Yamamoto-Taguchi N, et al. HTLV-1 bZIP factor induces inflammation through labile Foxp3 expression. *PLoS Pathog.* 2013;9(9):e1003630.
53. Shimoyama M. Diagnostic criteria and classification of clinical subtypes of adult T-cell leukaemia-lymphoma. A report from the Lymphoma Study Group (1984–1987). *Br J Haematol.* 1991;79(3):428–437.
54. Osame M. Review of WHO Kagoshima meeting and diagnostic guidelines for HAM/TSP. In: Blattner W, ed. *Human Retrovirology: HTLV*. New York, New York, USA: Raven Press; 1990:191–197.
55. Tanaka Y, et al. An antigenic structure of the trans-activator protein encoded by human T-cell leukemia virus type-I (HTLV-I), as defined by a panel of monoclonal antibodies. *AIDS Res Hum Retroviruses.* 1992;8(2):227–235.
56. Yoshiki T, et al. Models of HTLV-I-induced diseases. Infectious transmission of HTLV-I in inbred rats and HTVL-I env-pX transgenic rats. *Leukemia.* 1997;11(suppl 3):245–246.
57. Kamihira S, et al. Intra- and inter-laboratory variability in human T-cell leukemia virus type-1 proviral load quantification using real-time polymerase chain reaction assays: a multi-center study. *Cancer Sci.* 2010;101(11):2361–2367.
58. Bai Y, et al. Effective transduction and stable transgene expression in human blood cells by a third-generation lentiviral vector. *Gene Ther.* 2003;10(17):1446–1457.
59. Nagata K, Ohtani K, Nakamura M, Sugamura K. Activation of endogenous c-fos proto-oncogene expression by human T-cell leukemia virus type I-encoded p40tax protein in the human T-cell line, Jurkat. *J Virol.* 1989;63(8):3220–3226.
60. Dull T, et al. A third-generation lentivirus vector with a conditional packaging system. *J Virol.* 1998;72(11):8463–8471.
61. Shin HJ, Lee JB, Park SH, Chang J, Lee CW. T-bet expression is regulated by EGR1-mediated signaling in activated T cells. *Clin Immunol.* 2009;131(3):385–394.

Regular Article

LYMPHOID NEOPLASIA

The role of HTLV-1 clonality, proviral structure, and genomic integration site in adult T-cell leukemia/lymphoma

Lucy B. Cook,[1] Anat Melamed,[1] Heather Niederer,[1] Mikel Valganon,[2,3] Daniel Laydon,[1] Letizia Foroni,[2,3] Graham P. Taylor,[4] Masao Matsuoka,[5] and Charles R. M. Bangham[1]

[1]Section of Immunology, Wright-Fleming Institute, Imperial College, London, United Kingdom; [2]Imperial Molecular Pathology Laboratory, Imperial College Healthcare NHS Trust and Academic Health Sciences Centre, Hammersmith Hospital, London, United Kingdom; [3]Centre for Haematology, Faculty of Medicine, Imperial College, Hammersmith Hospital, London, United Kingdom; [4]Section of Virology, Wright-Fleming Institute, Imperial College, London, United Kingdom; and [5]Institute for Viral Research, Kyoto University, Kyoto, Japan

Key Points

- Adult T-cell leukemia (ATL) does not, as previously believed, result from the oligoclonal proliferation caused by HTLV-1 infection.
- In both ATL patients and those with nonmalignant infection, the HTLV-1 provirus preferentially survives in vivo in acrocentric chromosomes.

Adult T-cell leukemia/lymphoma (ATL) occurs in ~5% of human T-lymphotropic virus type 1 (HTLV-1)–infected individuals and is conventionally thought to be a monoclonal disease in which a single HTLV-1$^+$ T-cell clone progressively outcompetes others and undergoes malignant transformation. Here, using a sensitive high-throughput method, we quantified clonality in 197 ATL cases, identified genomic characteristics of the proviral integration sites in malignant and nonmalignant clones, and investigated the proviral features (genomic structure and 5′ long terminal repeat methylation) that determine its capacity to express the HTLV-1 oncoprotein Tax. Of the dominant, presumed malignant clones, 91% contained a single provirus. The genomic characteristics of the integration sites in the ATL clones resembled those of the frequent low-abundance clones (present in both ATL cases and carriers) and not those of the intermediate-abundance clones observed in 24% of ATL cases, suggesting that oligoclonal proliferation per se does not cause malignant transformation. Gene ontology analysis revealed an association in 6% of cases between ATL and integration near host genes in 3 functional categories, including genes previously implicated in hematologic malignancies. In all cases of HTLV-1 infection, regardless of ATL, there was evidence of preferential survival of the provirus in vivo in acrocentric chromosomes (13, 14, 15, 21, and 22). (*Blood.* 2014;123(25):3925-3931)

Introduction

Human T-lymphotropic virus type 1 (HTLV-1) causes adult T-cell leukemia/lymphoma (ATL) in approximately 5% of HTLV-1–infected individuals. A further ~5% of carriers develop an aggressive myelopathy known as HTLV-1–associated myelopathy (HAM) or other inflammatory diseases such as polymyositis. It remains uncertain why a minority develop aggressive clinical disease, typically decades following asymptomatic infection, whereas most infected individuals remain lifelong healthy carriers. The Shimoyama classification of ATL[1] contains 4 subtypes: acute, lymphoma, chronic, and smoldering. These subtypes differ in the response to treatment and overall survival, but little is known about either viral or host molecular determinants of disease. Several host cytogenetic or molecular defects have been described, but no recurrent genetic lesions have been identified.

The major predictor of clinical disease is the proviral load (PVL), the percentage of HTLV-1–infected peripheral blood mononuclear cells (PBMCs). The PVL remains relatively constant over years within an individual, rising slowly over decades.[2] However, the PVL varies widely between patients, ranging from <0.001% PBMCs to >100% (ie, >100 copies per 100 PBMCs); the risk of disease rises in carriers with a PVL >4% in Japan[3] and in those with a PVL >10% in the United Kingdom.[4] Nonetheless, there is overlap in the range of PVL seen between patients with disease and those that remain lifelong asymptomatic carriers, making individual patient prognosis difficult.

HTLV-1 appears to persist in chronic infection chiefly by mitotic proliferation of infected CD4$^+$ T cells, although the ratio of this mitotic spread to de novo infection[5] has not been rigorously estimated. Each clone of HTLV-1–infected cells can be identified by its particular integration site of the HTLV-1 provirus in the host genome[6]; the daughter cells of each clone share the same genomic integration site, and the frequency of these cells defines the abundance of a given clone. A majority of naturally infected cells in nonmalignant infection contain a single integrated provirus.[7]

ATL is characterized by monoclonal proliferation of CD4$^+$CD25$^+$ tumor cells. For many years, it has been believed that ATL arises following a steady progression from polyclonal infection of CD4$^+$ T cells to an oligoclonal expansion and, many years later, following a series of undefined genetic or epigenetic events, malignant transformation of a previously abundant clone to a monoclonal tumor. However, there are indications that HTLV-1 clonality in ATL may be

Submitted February 1, 2014; accepted April 3, 2014. Prepublished online as *Blood* First Edition paper, April 15, 2014; DOI 10.1182/blood-2014-02-553602.

A.M., H.N., and M.V. contributed equally to this study.

The online version of this article contains a data supplement.

The publication costs of this article were defrayed in part by page charge payment. Therefore, and solely to indicate this fact, this article is hereby marked "advertisement" in accordance with 18 USC section 1734.

more complex. One or more abnormally abundant clones may underlie the largest, putatively malignant clone,[6] and there are reports of "clonal succession" in which a malignant clone spontaneously regresses and an independent clone proliferates in its place.[8]

HTLV-1 expresses a transcriptional transactivator protein, Tax, which activates transcription of the HTLV-1 provirus and of many host genes[9]. Because Tax can immortalize rodent cells in vitro and Tax transgenic mice develop tumors, it has been widely accepted that Tax plays a role in leukemogenesis. This hypothesis is supported by the observations that Tax promotes DNA replication and cell-cycle progression, causes structural damage to host DNA, and inhibits DNA repair and cell-cycle checkpoints.[9] Tax expression is lost in ~40% of ATL cases, probably under selection from the strong anti-Tax cytotoxic T-lymphocyte (CTL) response,[10] but the relation between Tax expression and ATL subtype and progression is unclear. There is also increasing evidence that another HTLV-1 gene, *HBZ*, plays a critical part in leukemogenesis.[9]

To summarize, the molecular mechanisms of oncogenesis of ATL, and in particular the mechanisms and role of selective oligoclonal proliferation, are incompletely understood. Here, in a large cohort of ATL patients and geographically matched asymptomatic HTLV-1 carriers, we used a quantitative high-throughput sequencing approach to test the hypothesis that the genomic environment flanking the proviral integration site is associated with malignant transformation of HTLV-1–infected clones and correlated the findings with both the clinical subtype of ATL and genetic and epigenetic modifications of the HTLV-1 provirus.

Methods

Study subjects and control cell lines

Blood or lymph node samples were donated by 221 ATL patients and 75 asymptomatic HTLV-1 carriers (ACs) from the Kumamoto region of Japan, and DNA was extracted at the Institute for Viral Research, Kyoto University, Japan, with written consent in accordance with regulations defined by the Japanese Government and Kyoto University. This study was conducted in accordance with the Declaration of Helsinki. This study was approved by the UK National Research Ethics Service (reference 09/H0606/106). The chromosomal distribution of integration sites in the present cohort was compared with the distribution in samples from 2 previously described studies: individuals with natural (nonmalignant) HTLV-1 infection from Kagoshima, southern Japan,[11,12] and cells infected with HTLV-1 in vitro.[6,13] The rodent cell line Tarl2, containing a single copy of HTLV-1, was used for quantification of PVL. ATL control cell lines T-43 (methylated) and T-48 (unmethylated) were used as methylation controls.[14]

PVL quantification

PVL was measured by quantitative polymerase chain reaction (PCR) of *tax* and *actin* genes using ABI Fast SYBR green as per the manufacturer's protocol (Applied Biosystems), using PCR primers as previously described[15] and assuming a single copy of *tax*[7] and 2 copies of *actin* per cell. Thermal cycling conditions were 95°C for 20 seconds and 40 cycles each of 95°C for 1 second followed by 60°C for 20 seconds. Standard curves were generated using serial dilutions of the cell line Tarl2, as previously described.[6,13]

Long-range PCR to identify defective proviruses

An internal control region at the 3′ end of the HTLV-1 genome was amplified for each ATL case, followed by a long-range PCR to identify defective proviruses based upon the length of the long-range PCR product as published by Tamiya et al.[16] DNA was amplified using KOD Hot Start DNA polymerase (Toyoba, Novagen). Primers for the control PCR and cycling conditions were 5′-CTCTCACAGTGGGCTCGAGA-3′ and 5′-CAAAGACGTAGAGTT GAGCAAGC-3′, 95°C for 2 minutes, 30 cycles: 95°C for 20 seconds, 59°C for 10 seconds, and 70°C for 48 seconds, followed by 70°C for 5 minutes. The primers and cycling conditions for the long-range PCR were 5′-CTTAGAGCCTCCCAGTGAAAAACATTTCC-3′ and 5′-GATG CATGGTCCTGCAAGGATAACA-3′, 95°C for 2 minutes, 30 cycles: 95°C for 20 seconds, and 66°C for 175 seconds, followed by 72°C for 15 minutes. The PCR products were electrophoresed on a 1% agarose gel with expected product size of 2.85 kb for the control PCR and 6.5 kb for a complete long-range product. A long-range product shorter than 6.5 kb defines a type 1 defective provirus; failure to amplify any long-range product identifies a type 2 defective provirus.[16]

Exon 2 and exon 3 tax gene sequencing

Tax protein is 353 amino acids in length: exon 2 provides the methionine start codon, and the remaining amino acids are derived from exon 3. Exons 2 and 3 were sequenced in ATL samples with a complete provirus. Exon 2 was amplified using PCR products from long-range PCR using Phusion high-fidelity DNA polymerase (New England Biolabs [NEB]). Primers and cycling conditions were 5′-CCTCAGCAATAAACAAACCC-3′ and 5′-CAATTG TGAGAGTACAGCAG-3′, 98°C for 30 seconds, 20 cycles: 98°C for 5 s seconds, 51.5°C for 20 s seconds, and 72°C for 10 seconds, followed by 72°C for 5 minutes. PCR products were inspected on 2% agarose gel for product length (318 bp). Exon 3 was amplified from the control long-range PCR product using Phusion high-fidelity DNA polymerase (NEB). Primers and cycling conditions were 5′- ATACAAAGTTAACCATGCTT-3′ and 5′- AGACGTCAGAGCCTTAGTCT-3′, 98°C for 30 seconds, 20 cycles: 98°C for 5 seconds, 51.5°C for 10 seconds, and 72°C for 22 seconds, followed by 72°C for 5 minutes. PCR products were inspected on a 2% agarose gel for product length (1120 bp) and sequenced by Sanger sequencing using 6 different sequencing primers to capture the entire exon (5′-ATACAAAGTTAACCA TGCTT-3′, 5′-CGTTATCGGCTCAGCTCTACA-3′, 5′-TTCCGTTCC ACTCAACCCTC-3′, 5′- AGACGTCAGAGCCTTAGTCT-3′, 5′-GGGTT CCATGTATCCATTTC-3′, and 5′- GTCCAAATAAGGCCTGGAGT-3′).

Methylation-specific PCR (MS-PCR)

MS-PCR was undertaken on ATL samples with a complete provirus but without a nonsense mutation of the *tax* gene. Takeda et al[17] showed that MS-PCR correlates with bisulfite sequencing PCR and with the methylation status of the promoter/enhancer Tax-response element-1 in the 5′ long terminal repeat (LTR). DNA was treated overnight with sodium bisulfite (Sigma) and purified using Zymo EZ Bisulfite DNA cleanup as per the manufacturer's protocol (Zymo Research). DNA was amplified by heminested PCR using JumpStart RedTaq polymerase (Sigma). Primers for the first PCR reaction for methylated DNA were 5′-TTAAGTCGTTTTTAGGCGTTGAC-3′, 5′-AAA AAAATTTAACCCATTACC-3′ and for unmethylated DNA 5′- TTAA GTTGTTTTTAGGTGTTGAT-3′, 5′-AAAAAAATTTAACCCATTACC-3′. The thermal conditions for first PCR were 94°C for 2 minutes, 35 cycles: 94°C for 30 seconds, 53°C for 30 seconds, and 72°C for 2 minutes. Primers for the hemi-nested methylated PCR were 5′-GAGGTCGTTATTTACGTCGGTT GAGTC-3′, 5′-AAAAAAATTTAACCCATTACC-3′ and unmethylated PCR primers 5′-GAGGTTGTTATTTATGTTGGTTGAGTT-3′, 5′-AAAAAAA TTTAACCCATTACC-3′. The cycling conditions for the second PCR were 94°C for 2 minutes, 30 cycles: 94°C for 30 seconds, 57°C for 30 seconds, and 72°C for 2 minutes, followed by 72°C for 5 minutes. The PCR product was inspected on a 2% agarose gel for length (428 bp). MS-PCR primers did not amplify unconverted HTLV-1 or host genomic DNA.

T-cell receptor (TCR) gene rearrangement studies

TCR-γ gene rearrangement studies were undertaken in the Imperial Molecular Pathology Laboratory, Hammersmith Hospital (London, United Kingdom) using the established BIOMED-2 protocol followed by heteroduplex analysis and/or GeneScanning. GeneScan analysis was performed on an ABI 3130 genetic analyzer using GeneMapper 4.0 (Life Technologies).

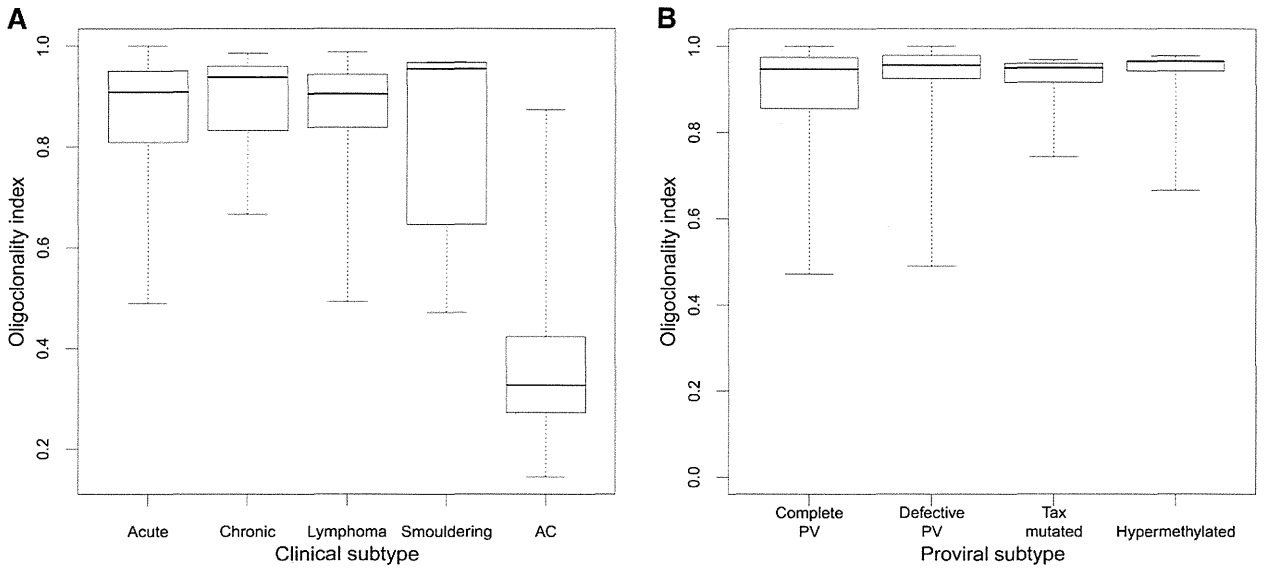

Figure 1. OCI by clinical and proviral subtype. (A) Median OCI of the ACs was 0.33 (range, 0.14-0.87), and median OCI for the ATL (all subtypes combined) was 0.91 (range, 0.47-1.0). There was no difference in OCI between ATL clinical subtypes. (B) There was no difference in OCI between the different mechanisms of proviral silencing. PV, provirus.

Integration site mapping and quantification

The high-throughput protocol for identification and quantification of proviral integration sites was carried out as previously described.[6] Mapped integration sites were compared with a set of randomly generated in silico genomic sites (n = 175 505) as previously reported.[13]

Bioinformatic annotation of genomic environment

Transcription units and cytosine guanine dinucleotide island data were retrieved from the National Center for Biotechnology Information (ftp.ncbi.nih.gov/gene/) and University of California, Santa Cruz tables, respectively. Epigenetic marks were annotated according to primary $CD4^+$ T-cell chromatin immunoprecipitation sequencing data published by Barski et al.[18] Transcription factor binding sites were obtained from published data sets (supplemental Figure 1 available at the *Blood* Web site) from chromatin immunoprecipitation sequencing experiments on primary human $CD4^+$ T cells or other primary human cells or cell lines, as previously described.[13] Cancer-associated gene data sets are defined by Sadelain et al.[19] Annotated genomic positions were compared with the integration site data using the hiAnnotator R package kindly provided by N. Malani and F. Bushman (University of Pennsylvania; http://malnirav.github.com/hiAnnotator).

Diversity estimator

The diversity estimator (DivE)[20] was used to estimate the total number of clones in addition to those observed. DivE involves fitting many mathematical models to nested subsamples of individual-based rarefaction curves. Estimates from the best-performing models are aggregated to produce the final estimate.[20] DivE requires an estimate of the number of cells in the blood; because the absolute PBMC count for each case was unknown, DivE estimates were calculated for each patient over 2 orders of magnitude of variation in the PBMC count (3×10^9/L, 50×10^9/L, and 500×10^9/L).

Statistical analysis

Statistical analysis was carried out using R version 2.15.2 (http://www.R-project.org/). The oligoclonality index (OCI; Gini coefficient)[6,21] was calculated using the R reldist package[22] (http://CRAN.R-project.org/package=reldist). Two-tailed nonparametric tests (Mann Whitney *U*, Fisher's exact, χ^2) were used for all comparisons. Bonferroni's correction for multiple testing was applied where appropriate. To test the hypothesis that 2 observed HTLV-1 integration sites were present in 1 T-cell clone, we used the Gaussian approximation to the binomial distribution (supplemental Figure 3). To identify clusters of integration sites or genomic hotspots of integration, we used R software developed by Presson et al[23] (http://www.biomedcentral.com/1471-2105/12/367). Functional categories of genes were analyzed through the use of Ingenuity Pathway Analysis (Ingenuity Systems; http://www.ingenuity.com).

Results

The ATL samples are derived from a representative cohort

We analyzed 197 cases of ATL; patients' characteristics are detailed in supplemental Figure 4. Systematic analysis of the proviral structure showed a complete provirus in 46% of cases, putatively capable of Tax expression; 39% of cases contained a defective provirus, 7% contained a nonsense mutation of the *tax* gene, and 8% contained a hypermethylated promoter in the 5′ LTR. There was no significant difference in OCI between ATL clinical subtypes (median OCI = 0.91) or by proviral subtype (median OCI = 0.91); the median OCI in asymptomatic carriers was 0.33, in the range previously reported[6] (Figure 1).

The median absolute number of $HTLV\text{-}1^+$ T-cell clones (estimated by the DivE technique) in the circulation in ACs was 9054. The median number of clones in the ATL cases was 1741 (assuming PBMC = 3×10^9/L) or 2154 (assuming PBMC = 50×10^9/L). These results show that although the white cell count may vary over an order of magnitude between individuals with ATL, the estimated number of distinct clones underlying the malignant clone remains relatively stable (~2000).

In 91% of ATL cases, a single copy of HTLV-1 is integrated into the host genome

In our protocol, the quasi-random DNA shearing by sonication allows unbiased, quantitative detection of proviruses[6,24] and therefore

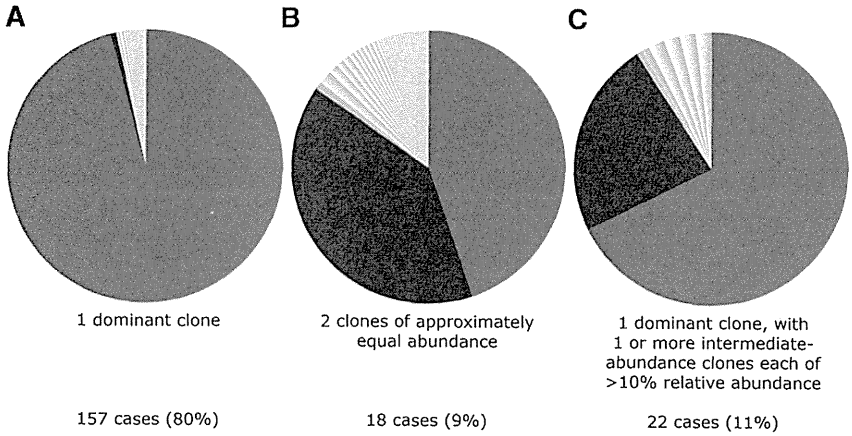

Figure 2. Examples of 3 typical clonal structures of ATL cases. Each sector in the pie charts depicts the relative abundance of the respective integration site. (A) Typical "monoclonal" ATL tumor sample; PVL = 63% (relative abundance of dominant clone = 97% of PVL). (B) Two equally abundant integration sites (relative abundance respectively 44% and 39% of PVL); PVL = 9%. (C) ATL with dominant clone and additional intermediate-abundance clone (relative abundance respectively 67% and 23% of PVL); PVL = 241%.

enabled us to quantify the presence of 2 abundant integration sites in an ATL tumor (Figure 2). In 157 out of 197 samples (80%), as expected, a single dominant proviral integration site was observed, with a median relative abundance of 99.4% of the PVL (range, 35% to 100%). However, in 40 out of 197 samples (20%), the presence of only a single provirus was less certain, because >1 abundant integration site was observed. In each of these 40 cases, there was 1 "large" ATL integration site with relative abundance >35% and an additional site with a relative abundance >10%. The question arises whether these represented 2 proviruses in 1 malignant clone or if there were 2 distinct abnormally expanded clones. If a single malignant clone contains 2 proviruses, then each will be present at the same frequency, assuming a steady kinetic state and no recent reinfection with a second provirus, and the clone will carry a single TCR gene rearrangement. Alternatively, if there are 2 large independent clones, then the 2 integration sites will differ in abundance and 2 distinct TCR gene rearrangements will be detected. We found no significant difference in the abundance of 2 integration sites in 18 cases (9.1% of cohort) (supplemental Figure 3), suggesting the presence of 2 proviruses in a single tumor clone. In 22 cases (11% of the cohort), we observed a large ATL clone and a second clone of abnormal but significantly lower abundance. TCR-γ gene rearrangement analysis of these 40 samples confirmed a monoclonal population in 7 out of 40 cases (3.1%); this technique may underestimate monoclonality, owing to the possibility of a second rearranged TCR-γ allele. To conclude, a single dominant provirus was detected in 91% of cases, whereas in 9% of tumors there was evidence of 2 proviruses. These results are consistent with the finding of multiple proviruses in 11% of cases reported by Tamiya et al[16] using low-throughput techniques.

Binning of clones into small, intermediate, or large

In subsequent analysis, each clone was binned according to its relative abundance, ie, the proportion of the subject's PVL occupied by that clone. Each ATL case contained at least 1 abundant clone with a relative abundance >35% (n = 217 clones) that was defined as large; "small" clones were defined as those of relative abundance <1% (n = 5925), and such clones constitute the great bulk of PVL in nonmalignant HTLV-1 infection.[6,13] Clones (n = 90) that constituted between 1% and 35% of PVL were classified as intermediate abundance. Clones (n = 16 909) identified in the AC cohort were analyzed together, because only 4 of these clones fulfilled the large-clone classification (supplemental Figure 2).

Large ATL clones have the same genomic characteristics as small (nonmalignant) clones, whereas intermediate-sized clones have unique genomic characteristics

The intermediate-abundance clones observed in 24% of cases (48/197) in addition to the large (presumed malignant) clone were larger (ie, had a greater absolute abundance) than any clones previously observed in AC or HAM/tropical spastic paraparesis cohorts.[6,13] Because progressive oligoclonal proliferation has been postulated to precede malignant transformation, we tested the hypothesis that there is a stepwise progression in the frequency of integration site characteristics from low-abundance clones through intermediate-abundance to large ATL clones. The results showed that the large, presumed malignant ATL clones had integration site characteristics indistinguishable from those of the low-abundance clones present in ACs and in patients with ATL. In contrast, the integration sites present in the intermediate-abundance clones in ATL patients, which are not observed in nonmalignant infection, differed from both the low- and high-abundance clones in each genomic attribute examined (Figure 3). Specifically, the intermediate-abundance clones lacked the associations observed in the ACs and in the low-abundance and high-abundance clones seen in ATL, with either transcriptional orientation or proximity to transcription start sites, cytosine guanine dinucleotide islands, or activatory epigenetic marks. Instead, the intermediate-abundance clones showed an association with proximity to inhibitory epigenetic marks (Figure 3C) and specific transcription-factor binding sites (TFBSs) within 100 bp upstream or downstream of the integration site, notably binding sites for P300/CBP-associated factor (odds ratio [OR] = 4.78), Rad 21 (part of the cohesin complex) (OR = 4.08), and ZNF263 (OR = 5.57). These effects disappeared at 1 kb from the integration site (Figure 3A). Integration in proximity to these specific TFBSs was identified in 8 out of 197 tumor samples (4.1% of cohort).

There are no hotspots of integration associated with large ATL clones

All data sets were further annotated to investigate the proximity of the integrated provirus to the nearest cancer-associated gene. The frequency of integration was significantly higher than random expectation within 10 kb of oncogenes in clones from ACs and low-abundance clones from ATL patients, and within 150 kb in the large ATL clones; this association was not observed in the intermediate-abundance clones. We conclude that integration in proximity to these cancer-related genes confers a survival advantage

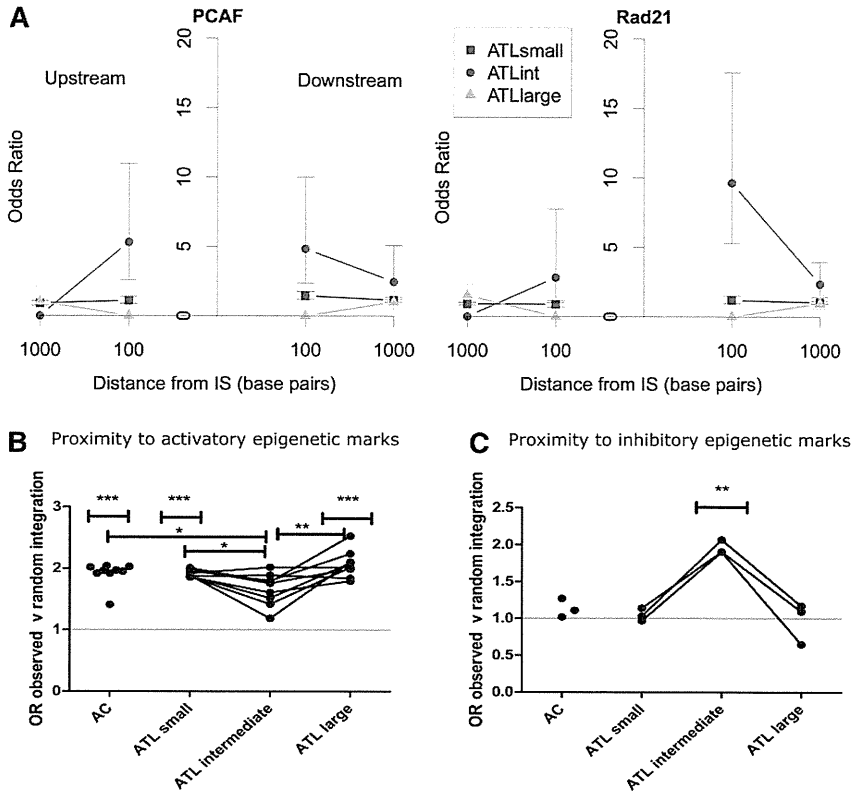

Figure 3. Intermediate-abundance clones in ATL cases contained proviruses with distinct genomic marks. (A) The OR of integration in proximity to specific TFBSs compared with AC is illustrated for 2 TFBSs, P300/CBP-associated factor binding sites (PCAFbsites) and Rad21. (See supplemental Figure 1 for full list of TFBSs tested). The y-axis shows the OR compared with ACs. The x-axis shows the distance in base pairs (logarithmic scale) from the integration site upstream (left-hand side) or downstream (right-hand side). "Upstream" and "downstream" are defined with respect to the sense strand of the HTLV-1 provirus. The junction of the x-axis and y-axis represents the integration site. There were no independent TFBS predictors for small clones (blue squares) or large clones (green triangles) in ATL cases compared with ACs (OR = 1) or when compared with each other or to random data sets (not illustrated). Independent TFBSs associated with intermediate-abundance clones in ATL cases (red circles) (PCAFbsites, Rad21) at 100 bp upstream or downstream compared with ACs are illustrated. (B) OR of integration in proximity to activatory epigenetic marks compared with random sites. AC, small, and large clones in ATL cases showed a significant bias toward integration in proximity to activatory epigenetic marks. There was no such bias in the intermediate-abundance clones. (C) OR of integration in proximity to inhibitory epigenetic marks compared with random. AC, small, and large clones in ATL cases showed no bias toward integration in proximity to inhibitory marks compared with random sites, whereas intermediate-abundance clones showed a bias toward inhibitory epigenetic marks (see supplemental Figure 1 for details of epigenetic marks tested). IS, integration site.

in vivo but does not play a significant role in leukemogenesis per se. The use of the powerful bioinformatic method of Presson et al[23] confirmed that there were no significant hotspots of integration associated with ATL.

The ontology of the nearest downstream gene was associated with the malignant clone in 6% of ATL cases

As a further test of the hypothesis that HTLV-1 proviral integration near host genes in a certain functional category confers a proliferative advantage on the infected T-cell clone, we used Ingenuity Pathway Analysis software to analyze the ontology of the nearest host genes upstream and downstream of each integration site. The results showed a significant overrepresentation of genes in 3 cellular pathways ("cell morphology," "immune cell trafficking," and "hematological system development and function") in the large ATL ("malignant") clones, but not in either the low- or intermediate-abundance clones (Figure 4). The 11 genes responsible for this significant association (*CD46*, *ITGA4*, *DPYSL2*, *RAP2A*, *CASP8*, *CDKN2A*, *GTF2I*, *TACR1*, *BCL2*, *IL6ST*, and *HGF*) accounted for 11 ATL cases (5.8% of the cohort) of different clinical subtypes. Furthermore, these effects were only seen in the nearest host gene downstream, regardless of its transcriptional orientation relative to the provirus. The median distance from the integration site to these nearest genes was 13.7 kb (range, 0.6-294 kb) compared with a median distance of 122.3 kb from all integration sites to the nearest cancer-associated gene ($P = .009$, Mann Whitney U test).

The HTLV-1 provirus preferentially survives in acrocentric chromosomes in vivo

Meekings et al[25] reported that the frequency of HTLV-1 proviruses in chromosome 13 was significantly higher in vivo than expected by chance, but the biological significance of this observation was uncertain. Here, using our quantitative, high-throughput technique, we observed a significant excess of integrations in chromosomes 13, 14, 15, and 21 compared with random and in vitro data sets. This excess was seen in all infected individuals and was not confined to those with ATL. There was a trend toward excess integrations in chromosome 22, but this was not statistically significant (Figure 5). These findings were validated with a second cohort of independent AC samples from the Kagoshima region of Japan. The chromosomal distribution of proviruses in the intermediate-abundance and large ATL clones was not significantly different from random, perhaps because of the small number of clones (n = 307).

Discussion

Oligoclonal proliferation of HTLV-1–infected T-cells is a cardinal feature of HTLV-1 infection. It has long been believed that this oligoclonal proliferation is primarily responsible for maintaining the high PVL of HTLV-1, which is the strongest correlate of risk of both the inflammatory (HAM) and malignant (ATL) diseases. However, we recently showed that the PVL correlates with the total number of infected clones, but not with the degree of oligoclonal proliferation as measured by the OCI.[6,13] Here, we show that ATL is frequently accompanied by a population of abnormally abundant HTLV-1–infected T-cell clones underlying the largest, putatively malignant clone. This observation suggested that such intermediate-abundance clones might represent an intermediate stage of malignant transformation between the low-abundance clones and the fully transformed, largest clone. However, we found that the host genomic attributes of the integration site in the large ATL clones closely

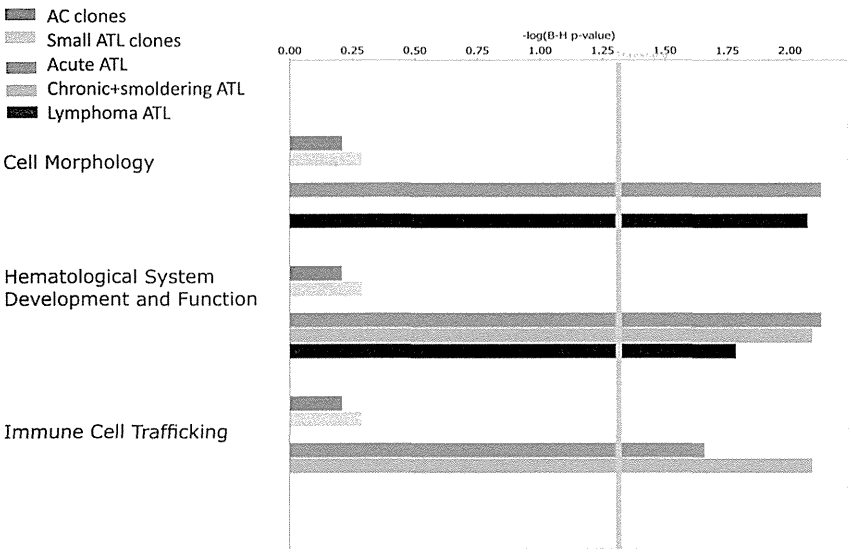

Figure 4. Functional classification of gene ontologies overrepresented among the large ATL clones. Functional categories significantly overrepresented among the random, AC, ATL small, intermediate, and large ATL clones as analyzed by Ingenuity software using the Ingenuity Pathways Knowledge Base (IPKB) gene population as baseline. Horizontal bars are only visible where there was a statistical overrepresentation of the pathway compared with the IPKB. Because there were no overrepresented pathways involving the random integration sites or intermediate-abundance clones in ATL cases, the bars are not visible. The vertical yellow threshold represents the line of statistical significance ($P < .05$) after correction (Benjamini-Hochberg) for multiple testing. The numbers of searchable genes for comparison with the IPKB were random (n = 96 706), AC (n = 5679), ATL small (n = 1628), ATL intermediate (n = 87), or ATL large (acute n = 141, lymphoma n = 31, chronic and smoldering n = 38).

resembled those of the low-abundance clones present both in ATL patients and in those with nonmalignant infection, whereas the integration site characteristics of the intermediate-abundance clones differed from both the low- and high-abundance clones and from the clones observed in nonmalignant cases of HTLV-1 infection. We conclude that the malignant clone does not arise from the intermediate-abundance clones but instead from the low-abundance clones. This conclusion is consistent with the observations that the low-abundance clones constitute the bulk of the PVL in HTLV-1 infection[6] and that the risk of ATL is correlated with the PVL.[2,4] We have also observed cases in which the malignant clone emerges from the large population of low-abundance clones, not from the preexisting oligoclonally expanded population.[26] Finally, this conclusion is also consistent with our recent observation[27] of highly oligoclonal proliferation and a small total number of clones in human T-lymphotropic virus type 2 infection, which does not cause malignant disease.

We therefore propose that the major determinant of the risk of ATL is the absolute number of clones: the larger the number, the greater the chance of malignant transformation. It is likely that the number of HTLV-1–infected clones present in an individual during chronic infection is determined chiefly by the efficiency of the host's CTL response to the virus, which in turn is determined by the HLA and killer immunoglobulin-like receptor genotype.[10,28]

The observation that the abnormally expanded intermediate-abundance clones seen in patients with ATL do not share genomic characteristics with either the polyclonal background or the malignant clones suggests that the intermediate-abundance clones arise as a consequence of ATL development and are not causative. One possibility is that these clones survive and proliferate as a consequence of the severely impaired immune response in ATL. The malignant clones in ATL use well-described mechanisms to silence Tax, either before or after malignant transformation, which allows them to escape the immunodominant CTL response and so confers a survival advantage. Once the malignant clone has emerged, the resulting immune impairment may allow the intermediate-abundance clones to survive despite continued expression of viral genes.

As expected, we did not identify any hotspots of integration, although analysis of the ontology of flanking genes demonstrated a functional overrepresentation of certain genes that are known to be dysregulated in many leukemias. This effect was significant only in the large (presumed malignant) ATL clones and only when considering the ontology of the nearest host gene downstream; there was no effect of the upstream host gene. Further, these specific genes lay very close (median 13.7 kb) to the provirus, suggesting a mechanistic interaction between the provirus and the downstream gene. Although the associations reported here between ATL and individual genes and genomic features account for a small proportion of the observed cases of ATL, these results indicate that transcriptional interactions between the provirus and the flanking host genome influence the risk of malignant transformation. Vogelstein recently estimated that each tumor-driver mutation contributes a survival advantage of ~0.4% to

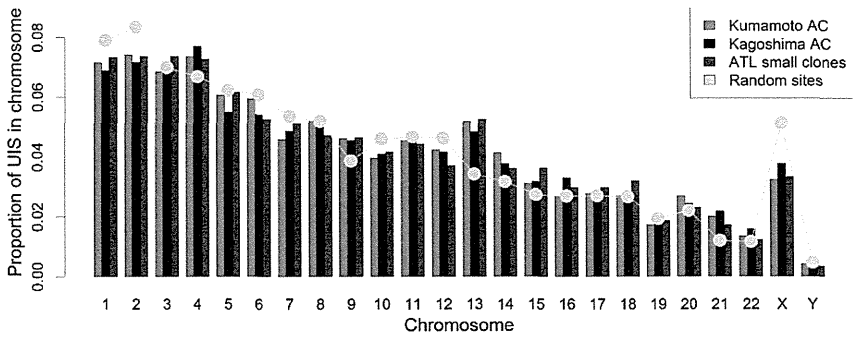

Figure 5. Preferential survival of HTLV-1 in vivo in chromosomes 13, 14, 15, and 21. The proportion of unique integration sites (UIS) per chromosome is shown for 2 independent AC data sets (Kumamoto and Kagoshima) and the small clones in ATL cases. The yellow line shows the frequency of sites in the random data set. There were an increased number of integrations in chromosomes 13, 14, 15, and 21 in the clones of asymptomatic carriers and small clones in ATL cases compared with random. The bias remained in chromosomes 13 and 15 when compared with a previously reported data set[6] of integration sites from Jurkat cells infected in vitro with HTLV-1.